



Harmonized gap-filled datasets from 20 urban flux tower sites

Mathew Lipson^{1,2}, Sue Grimmond², Martin Best³, Winston Chow⁴, Andreas Christen⁵, Nektarios Chrysoulakis⁶, Andrew Coutts⁷, Ben Crawford⁸, Stevan Earl⁹, Jonathan Evans¹⁰, Krzysztof Fortuniak¹¹, Bert G. Heusinkveld¹², Je-Woo Hong¹³, Jinkyu Hong¹⁴, Leena Järvi¹⁵, Sungsoo Jo¹⁶, Yeon-Hee Kim¹⁷,
5 Simone Kotthaus¹⁸, Keunmin Lee¹⁹, Valéry Masson²⁰, Joseph P. McFadden²¹, Oliver Michels²²,
Włodzimierz Pawlak²³, Matthias Roth²⁴, Hirofumi Sugawara²⁵, Nigel Tapper²⁶, Erik Velasco²⁷, Helen
Claire Ward²⁸

- ¹Australian Research Council (ARC) Centre of Excellence for Climate System Science, Climate Change Research Centre,
10 Level 4, Mathews Building, UNSW Sydney, New South Wales, 2052, Australia.
²Department of Meteorology, University of Reading, Reading, RG6 6ET, United Kingdom
³Met Office, Fitzroy Road, Exeter, Devon, EX1 3PB, United Kingdom.
⁴School of Social Sciences, Singapore Management University, Singapore.
⁵Environmental Meteorology, Institute of Earth and Environmental Sciences, Faculty of Environment and Natural
15 Resources, University of Freiburg, Freiburg, Germany.
⁶Foundation for Research and Technology Hellas, Institute of Applied and Computational Mathematics, Remote Sensing
Lab, Heraklion, Greece.
⁷School of Earth, Atmosphere and Environment, Monash University, Melbourne, Australia.
⁸Geography and Environmental Sciences, University of Colorado, Denver, Colorado, USA.
20 ⁹Global Institute of Sustainability and Innovation, Arizona State University, Tempe, Arizona, USA.
¹⁰UK Centre for Ecology & Hydrology, Crowmarsh Gifford, Wallingford, United Kingdom.
¹¹Department of Meteorology and Climatology, University of Lodz, Lodz, Poland.
¹²Department of Meteorology and Air Quality, Wageningen University, The Netherlands.
¹³Korea Environment Institute, Sejong, Republic of Korea.
25 ¹⁴Ecosystem-Atmosphere Process Lab, Department of Atmospheric Sciences, Yonsei University, Seoul, Korea (Republic of).
¹⁵Institute for Atmospheric and Earth System Research/Physics, Faculty of Science, University of Helsinki, Helsinki,
Finland.
¹⁶Ecosystem-Atmosphere Process Lab, Department of Atmospheric Sciences, Yonsei University, Seoul, Korea (Republic of).
¹⁷National Institute of Meteorological Sciences, Korea Meteorological Administration, Jeju, Korea (Republic of).
30 ¹⁸Institut Pierre Simon Laplace (IPSL), CNRS, École Polytechnique, Institut Polytechnique de Paris, 91128 Palaiseau Cedex,
France.
¹⁹Ecosystem-Atmosphere Process Lab, Department of Atmospheric Sciences, Yonsei University, Seoul, Republic of Korea.
²⁰Centre National de Recherches Météorologiques, University of Toulouse, Météo-France and CNRS, Toulouse, France.
²¹Department of Geography and Earth Research Institute, University of California, Santa Barbara, United States.
35 ²²Environmental Meteorology, Albert-Ludwigs-University, Freiburg, Germany.
²³Department of Meteorology and Climatology, University of Lodz, Lodz, Poland.
²⁴Department of Geography, National University of Singapore, Singapore.
²⁵National Defense Academy of Japan.
²⁶School of Earth, Atmosphere and Environment, Monash University, Melbourne, Australia.
40 ²⁷Independent Research Scientist, Singapore.
²⁸Department of Atmospheric and Cryospheric Sciences, University of Innsbruck, Innsbruck, Austria.

Correspondence to: Mathew J. Lipson (mathew.lipson@unsw.edu.au)



Abstract. Twenty urban neighbourhood-scale eddy covariance flux tower datasets have been harmonized and quality controlled, producing a 50 site-year collection with broad diversity in climate and urban surface characteristics. Observations are gap-filled and prepended with 10 years of reanalysis-derived local data to enable use as spin up and forcing for land surface model evaluation. For both gap filling and spin-up, ERA5 reanalysis meteorological data are bias corrected using tower observations, accounting for diurnal, seasonal and local urban effects not modelled in ERA5. The bias correction methods developed perform well compared to methods used in other datasets (e.g. WFDE5 or FLUXNET2015). Site description metadata includes local land cover fractions (buildings, roads, trees, grass etc.), building height and morphology, aerodynamic roughness estimates, population density and satellite imagery. Together, this collection can help extend our understanding of urban environmental processes through observational synthesis studies or in the evaluation of land surface environmental models in a wide range of urban settings.

1 Background

Tower mounted instruments allow the measurement of land-atmosphere fluxes (e.g. energy, momentum, water, carbon) and local meteorological conditions. These observations are one of the fundamental ways of improving both our understanding and ability to predict biogeophysical and weather-related processes at local scales. Regional and global networks of flux tower sites have helped extend our knowledge of ecosystem and climate science (Novick et al., 2018; Beringer et al., 2016; Yamamoto et al., 2005; Valentini, 2003). Over the last 25 years networks such as FLUXNET have progressively increased access to flux data through open-source collections (Pastorello et al., 2020), extending the reach and impact of individual site observations through synthesis studies (Baldocchi, 2020) and multi-site environmental modelling and model evaluation projects (Best et al., 2015; Ukkola et al., 2022). However, with few urban sites included, urban areas have not benefited from the improved understanding or more extensive model evaluations that these collections can facilitate.

Urban areas are unique ecosystems, distinct from natural or rural landscapes. First, most people live in cities (UN, 2018) and infrastructure is concentrated within them. Therefore, climate-related health and economic impacts fall disproportionately within urban areas. Second, urban infrastructure (e.g. buildings and roads) along with transient human activities (e.g. energy consumption and irrigation) fundamentally alter surface energy, water and mass exchanges with the atmosphere, modifying local and larger-scale environmental conditions (Oke et al., 2017). Third, as built environments, urban areas are uniquely capable of actively mitigating and adapting to climate change.

Establishing and maintaining long term flux sites in cities is particularly challenging because of the rarity of appropriate sites with homogenous fetch, the difficulty in gaining approval to access existing towers (e.g. for telecommunications), the cost of constructing tall towers over an aerodynamically rough surface, and extremely limited long-term funding opportunities (Arnfield, 2003; Grimmond, 2006; Velasco and Roth, 2010; Feigenwinter et al., 2012; Grimmond and Ward, 2021). Thus, despite the diversity and importance of urban areas across the globe, urban flux tower data are relatively scarce, generally of



short duration and rarely open source. Databases identifying urban observational programmes exist (e.g. the Urban Flux
75 Network (Grimmond and Christen, 2012)), however urban flux tower datasets have not previously been brought together into
a harmonised, gap-filled, open access collection.

We bring together quality-controlled data from 20 urban sites in an open collection that includes 50 observation-years (Lipson
et al., 2022). The sites are chosen to be diverse in both regional climates and urban characteristics. As evaluating land surface
models is one key application for these data, we create continuous forcing data sets (i.e. with incoming radiation fluxes and
80 other meteorological data) that are gap filled using site specific, bias corrected reanalysis data. Observations are also prepended
with 10 years of site-specific reanalysis-derived meteorological data to allow modelled soil moisture and other conditions to
equilibrate with local climate conditions during model spin up.

Along with the meteorological data, site characteristics and metadata are provided in a common format. The metadata includes
tower location, land cover fractions, building heights and morphology, aerodynamic roughness parameter estimates, population
85 density, estimated anthropogenic heat fluxes, site photos and satellite imagery. Together, this collection can help extend our
understanding of urban environmental processes through observational synthesis studies, or in the evaluation of land surface
environmental models in different urban settings.

2 Methods

2.1 Site selection

90 The initial motivation for collating these flux tower and site data is for use in the Urban-PLUMBER multi-site model evaluation
project, currently underway (Urban-PLUMBER: A multi-site model evaluation project for urban areas - Project Home, 2021).
Urban-PLUMBER draws on methods from the first international urban land surface model comparison (Grimmond et al.,
2010, 2011) and the Protocol for the Analysis of Land Surface Models Benchmarking Evaluation Project (PLUMBER (Best
et al., 2015)). The latter evaluated land surface models in non-urban (vegetated) areas, while Urban-PLUMBER evaluates land
95 surface models at 20 urban sites (Fig. 1, Table 1).

There is a two-fold use of these observational data in the model evaluation of Urban-PLUMBER:

1. To provide local-scale meteorological input forcing to drive land surface models
2. To evaluate the performance of models, primarily assessing the local-scale exchange of radiant and turbulent heat
fluxes between the surface and lower atmosphere

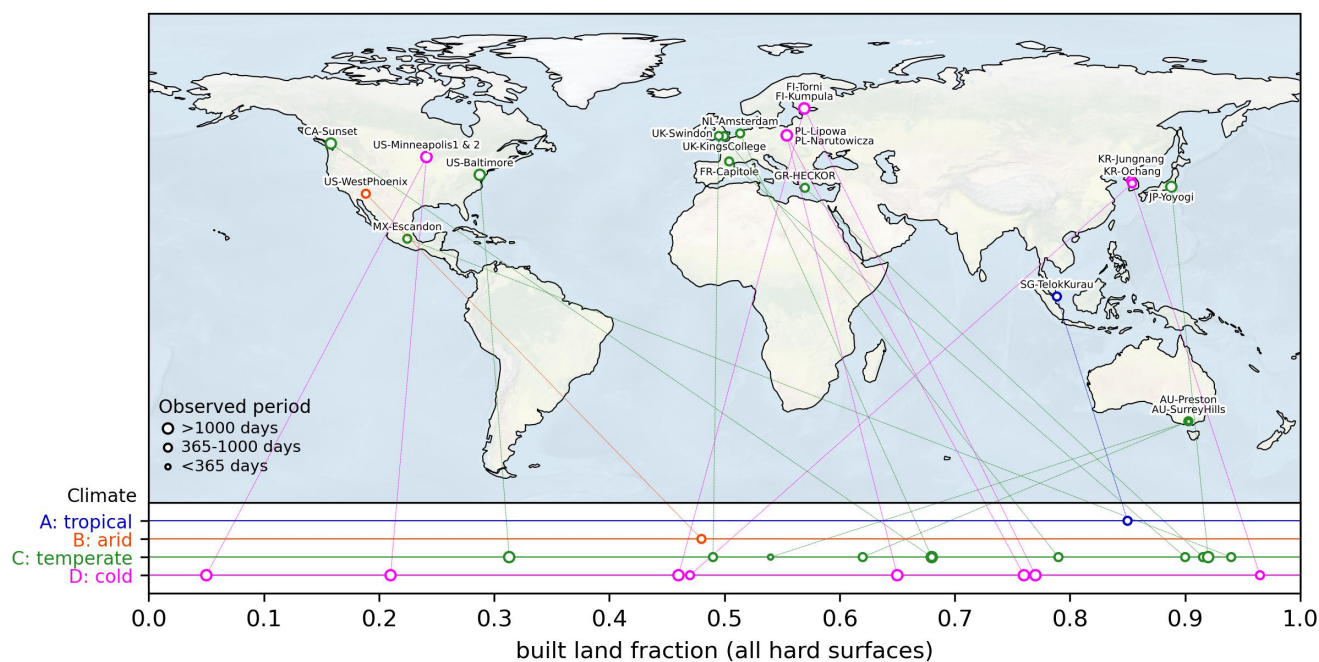
100 With these objectives in mind, the following criteria are used to select flux tower sites:

- Appropriately sited for neighbourhood-scale conditions - i.e. within the inertial sub-layer, typically 2-5 times above
the average building height and with relatively homogenous fetch (Grimmond, 2006; Barlow, 2014; Grimmond and
Ward, 2021)



105

- Requested observations available at 30- or 60-minute resolution (Table 2)
- Local site characteristics available for description and configuring models
- A preference for longer datasets (as this allows seasonal and inter-annual variability to be included)
- Collectively represent a diverse range of site characteristics and climates



110

Figure 1: Location of flux tower sites in this collection. Each site Köppen-Geiger climate classification (Beck et al., 2018) and the built land fraction around the tower are indicated at the bottom of the figure.

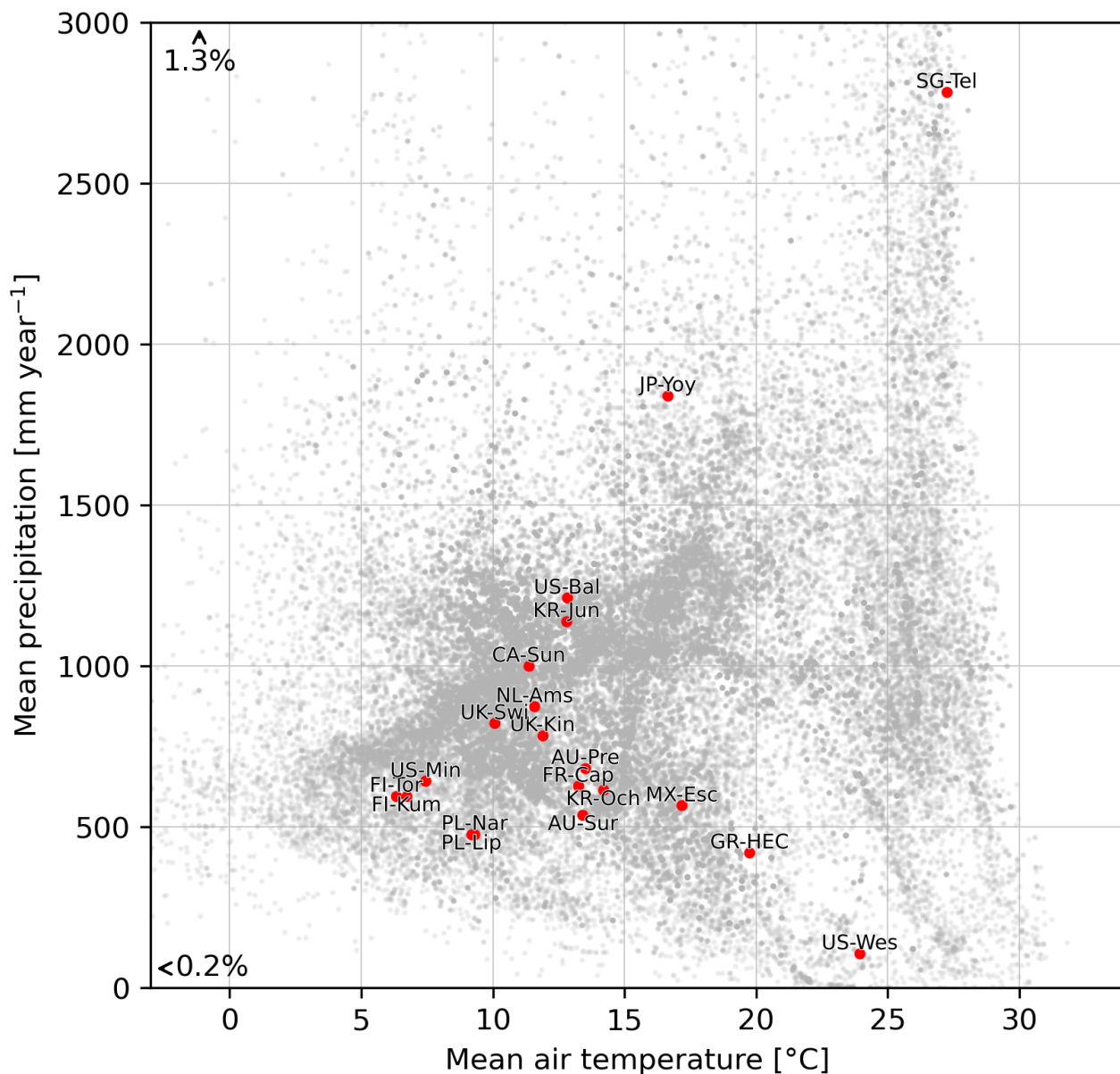
Table 1: Site location and included observation (focus) period. Data providers may have longer observation periods available than are in this collection. Resolution is 30 minutes (or 60 minutes if denoted by *). All periods in universal time coordinated (UTC). US-Minneapolis data are split based on wind direction and fetch (Section 4.5).

Sitename	City	Country	Observed period	Latitude	Longitude	References
AU-Preston	Melbourne	Australia	Aug 2003 – Nov 2004	-37.7306	145.0145	(Coutts et al., 2007a, b)
AU-SurreyHills	Melbourne	Australia	Feb 2004 – Jul 2004	-37.8265	145.099	(Coutts et al., 2007a, b)
CA-Sunset	Vancouver	Canada	Jan 2012 – Dec 2016	49.2261	-123.078	(Christen et al., 2011; Crawford and Christen, 2015)
FI-Kumpula	Helsinki	Finland	Dec 2010 – Dec 2013	60.2028	24.9611	(Karsisto et al., 2016)
FI-Torni	Helsinki	Finland	Dec 2010 – Dec 2013	60.1678	24.9387	(Järvi et al., 2018; Nordbo et al., 2013)
FR-Capitole	Toulouse	France	Feb 2004 – Mar 2005	43.6035	1.4454	(Masson et al., 2008; Goret et al., 2019)
GR-HECKOR	Heraklion	Greece	Jun 2019 – Jun 2020	35.3361	25.1328	(Stagakis et al., 2019)
JP-Yoyogi	Tokyo	Japan	Mar 2016 – Mar 2020*	35.6645	139.6845	(Hirano et al., 2015; Ishidoya et al., 2020)
KR-Jungnang	Seoul	South Korea	Jan 2017 – Apr 2019	37.5907	127.0794	(Jo et al., n.d.; Hong et al., 2020)
KR-Ochang	Ochang	South Korea	Jun 2015 – Jul 2017	36.7197	127.4344	(Hong et al., 2019, 2020)
MX-Escandon	Mexico City	Mexico	Jun 2011 – Sep 2012	19.4042	-99.1761	(Velasco et al., 2011, 2014)
NL-Amsterdam	Amsterdam	Netherlands	Jan 2019 – Oct 2020	52.3665	4.8929	-



PL-Lipowa	Łódź	Poland	Jan 2008 – Dec 2012*	51.7625	19.4453	(Fortuniak et al., 2013; Pawlak et al., 2011)
PL-Narutowicza	Łódź	Poland	Jan 2008 – Dec 2012*	51.7733	19.4811	(Fortuniak et al., 2013, 2006)
SG-TelokKurau06	Singapore	Singapore	Apr 2006 – Mar 2007	1.3143	103.9112	(Roth et al., 2017)
UK-KingsCollege	London	UK	Apr 2012 – Jan 2014	51.5118	-0.1167	(Bjorkegren et al., 2015; Kotthaus and Grimmond, 2014a, b)
UK-Swindon	Swindon	UK	May 2011 – Apr 2013	51.5846	-1.7981	(Ward et al., 2013)
US-Baltimore	Baltimore	USA	Jan 2002 – Jan 2007*	39.4128	-76.5215	(Crawford et al., 2011)
US-Minneapolis	Minneapolis	USA	Jun 2006 – May 2009	44.9984	-93.1884	(Peters et al., 2011; Menzer and McFadden, 2017)
US-WestPhoenix	Phoenix	USA	Dec 2011 – Jan 2013	44.9984	-93.1884	(Chow, 2017; Chow et al., 2014)

- Potential sites identified from published site lists (Grimmond and Christen, 2012; Oke et al., 2017) and open calls for data (e.g. community newsletters (Lipson et al., 2020a), international conferences (Lipson et al., 2020b, c) and social media professional networks). We deemed 20 sites sufficient for the evaluation project (Table 1), together covering a 50 site-years. Included sites have built fractions (i.e. plan area fraction of all impervious surfaces including roofs, roads, other paving *etc.*) from 0.05 to 0.965, and are located in four major Köppen-Geiger (Beck et al., 2018) climate classes (Fig. 1). Eleven sites are in temperate climates, eight in cold (or continental) climates, and one in each of tropical and arid climates.
- Sites are reasonably distributed across mean temperature and precipitation for global urban locations, but gaps remain, particularly in warm, wet and very cold climates (Fig. 2). Some urban flux observations in understudied regions were not included (e.g., Ouagadougou (Offerle et al., 2005), São Paulo (Ferreira et al., 2013), Guangzhou (Shi et al., 2019), Beijing (Dou et al., 2019)) because they do not meet the model evaluation project needs because of the relatively short observed periods for the available data. These regions and climates have large urban populations with significant environmental challenges and have few urban flux tower sites compared with northern hemisphere temperate or continental locations (Grimmond, 2006; Roth et al., 2017). Understudied regions and climates should be included in future collections when appropriate time series become available.



130 **Figure 2:** Climatology of included sites compared with more than 70,000 global urban areas. Mean temperature and annual precipitation at the 20 tower sites (red, truncated site name, Table 1) from tower observations; global urban locations (grey) from ERA5 surface data (Hersbach et al., 2020, 2018) (2000 – 2010) from grid nearest to locations identified in the Global Rural-Urban Mapping Project (GRUMP) (Center for International Earth Science Information Network - CIESIN - Columbia University et al., 2017). Locations with rainfall above 3000 mm year⁻¹ (1.3% of locations), and mean temperature below -3°C (0.2 % of locations) are not shown.



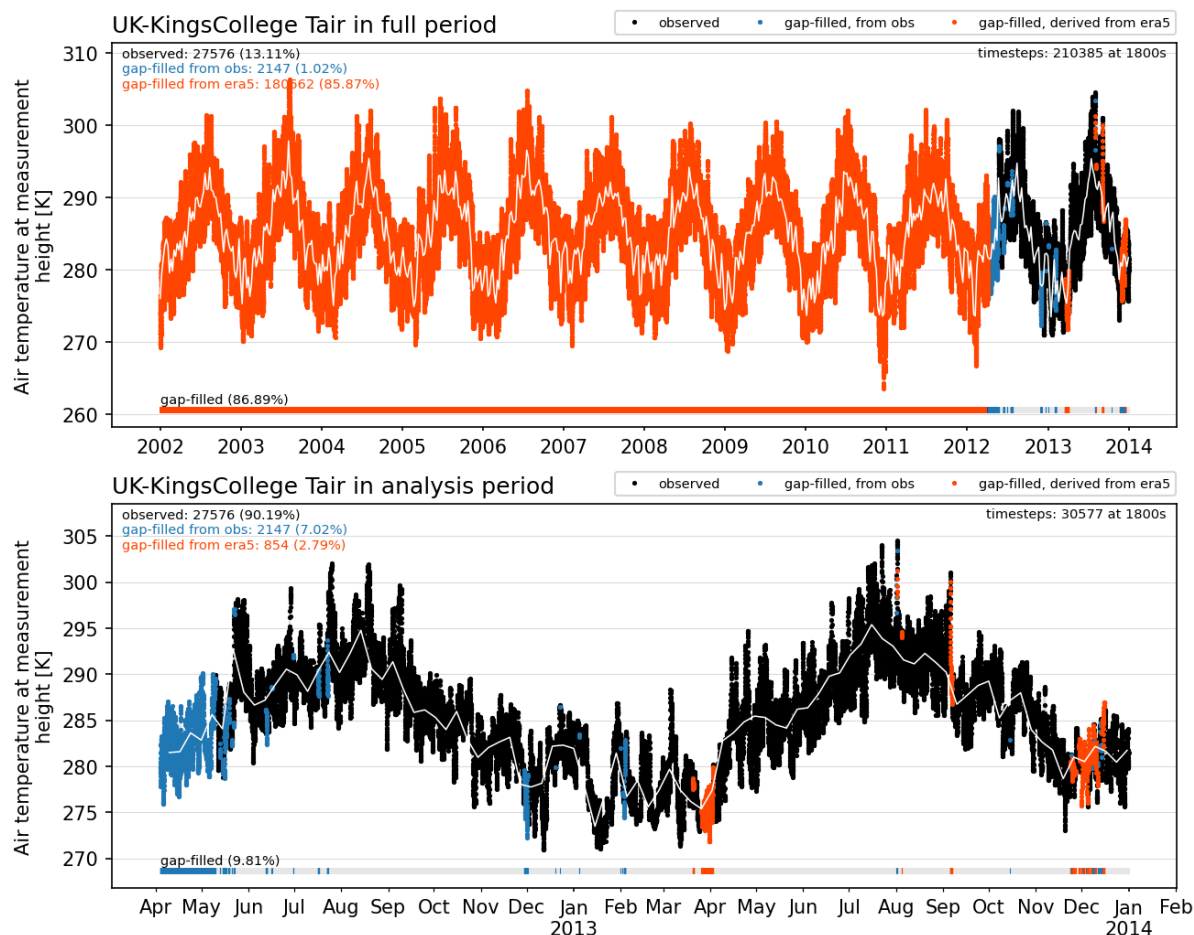
135 2.2 Flux tower data

The observed data are provided in 30- or 60-minute periods (Table 1), processed from high-frequency samples by individual observing groups. In the harmonized collection time stamps are in coordinated universal time (UTC) indicating the end of the measurement period. Variables name and units use ALMA conventions: (Assistance for Land-surface Modelling Activities), a format used in previous land surface model comparisons.

140 Data are cleaned (Sect 2.3: *Quality control*), gap filled (Section 2.4) and prepended with data derived from ERA5 (Section 2.5:) after site-specific corrections (Section 2.6). An example of final prepended and gap-filled data is shown in Figure 3 for one site (UK-KingsCollege). Plots for all other variables and sites are also available in the collection (Lipson et al., 2022).

Data are split into forcing and analysis variable sets (Table 2) to allow the forcing variables to be provided to modelling groups as input to run their models. The withheld analysis data are used by the coordinating group to assess the model outputs.

145 Some additional observed variables (Table 3) have, where practical, been included in the datasets after passing through the quality control steps. Missing forcing variables are obtained using bias-corrected reanalysis data (Section 2.4). No gap filling is applied to analysis data or additional variables.



150 **Figure 3:** Forcing timeseries with gap filling. Example shown for air temperature (T_{air}) at Kings College, London (UK-KingsCollege); (a) full forcing period, including 10 years of ERA5-derived data (red) prior to observations (black) used for model spin up, and (b) focus period used for analysis. Gaps are first filled from nearby tower measurements where available, and short gaps (≤ 2 hours) are linearly interpolated (blue). Remaining gaps are filled using the ERA5-derived timeseries which is seasonally and diurnally bias corrected using site observations. White lines show seven day mean values. Similar plots are available for other sites within the site data collection (Lipson et al., 2022).

155 **Table 2:** Forcing and analysis flux tower data variables. Short name description, units and positive direction use ALMA data conventions. Mean annual estimates of anthropogenic heat flux are included as site metadata. Note ground heat flux (Q_g) is the heat flux into soil rather than total storage heat flux which is difficult to measure in urban areas (Grimmond and Oke, 1999).

Variable	Description	Units	Positive direction	ERA5 bias correction
Forcing data				
SWdown	Downward shortwave radiation	$W m^{-2}$	Downward	none
LWdown	Downward longwave radiation	$W m^{-2}$	Downward	hourly and daily
Tair	Air temperature	K	-	hourly and daily
Qair	Specific humidity	$kg kg^{-1}$	-	hourly and daily
PSurf	Station air pressure	Pa	-	hourly and daily
Wind_N	Northward wind component	$m s^{-1}$	Northward	logarithmic law
Wind_E	Eastward wind component	$m s^{-1}$	Eastward	logarithmic law



Variable	Description	Units	Positive direction	ERA5 bias correction
Forcing data				
Rainf	Rainfall rate	kg m ⁻² s ⁻¹	Downward	long term precipitation
Snowf	Snowfall rate	kg m ⁻² s ⁻¹	Downward	long term precipitation
Analysis data				
SWup	Upward shortwave radiation	W m ⁻²	Upward	none
LWup	Upward longwave radiation	W m ⁻²	Upward	none
Qle	Latent heat flux	W m ⁻²	Upward	none
Qh	Sensible heat flux	W m ⁻²	Upward	none
Additional data (optional)				
Qg	Ground heat flux into soil	W m ⁻²	Downward	none
Qtau	Momentum flux	N m ⁻²	Downward	none
Tair2m	Near surface air temperature (2 m)	K	-	none
SoilTemp	Soil temperature (depth in metadata)	K	-	none

Table 3: Site climate classification, missing and additional variables. Climate classification from Köppen-Geiger global dataset (Beck et al., 2018). Table 2 gives variable definitions. Note: as MX-Escandon LWdown data are unavailable during the 2011-2012 focus period, but were available in 2006, this earlier period is used to determine bias correction for ERA5 LWdown data.

160

Sitename	Class	Climate description	Missing variables	Additional variables
AU-Preston	Cfb	Temperate, no dry season, warm summer	Snowf	Qtau
AU-SurreyHills	Cfb	Temperate, no dry season, warm summer	Snowf	Qtau
CA-Sunset	Csb	Temperate, dry summer, warm summer	Snowf	Qtau, SoilTemp
FI-Kumpula	Dfb	Cold, no dry season, warm summer	Snowf	
FI-Torni	Dfb	Cold, no dry season, warm summer	Snowf	
FR-Capitole	Cfa	Temperate, no dry season, hot summer	Snowf	Qtau
GR-HECKOR	Csa	Temperate, dry summer, hot summer	Snowf	Qtau
JP-Yoyogi	Cfa	Temperate, no dry season, hot summer		
KR-Jungnang	Dwa	Cold, dry winter, hot summer	Snowf	
KR-Ochang	Dwa	Cold, dry winter, hot summer	Snowf	
MX-Escandon	Cwb	Temperate, dry winter, warm summer	Snowf, LWdown*	Qtau
NL-Amsterdam	Cfb	Temperate, no dry season, warm summer	Snowf	Qtau
PL-Lipowa	Dfb	Cold, no dry season, warm summer	Snowf	
PL-Narutowicza	Dfb	Cold, no dry season, warm summer	Snowf	
SG-TelokKurau06	Af	Tropical, rainforest	Snowf	
UK-KingsCollege	Cfb	Temperate, no dry season, warm summer	Snowf	Qtau
UK-Swindon	Cfb	Temperate, no dry season, warm summer	Snowf	Qtau
US-Baltimore	Cfa	Temperate, no dry season, hot summer	Snowf	Qtau, SoilTemp
US-Minneapolis	Dfa	Cold, no dry season, hot summer	Snowf	Qtau, SoilTemp, Qg
US-WestPhoenix	BWh	Arid, desert, hot	Snowf	Qtau, SoilTemp

2.3 Quality control and assurance

For each site the 30- or 60-minute variables are calculated by data providers from high-frequency samples after applying their own quality control measures (e.g. Aubinet et al., 2012; Feigenwinter et al., 2012; Kotthaus and Grimmond, 2012; Vitale et al., 2020). The harmonised collection consists of the data retained after undergoing five additional quality control steps, in this order:

165



1. **Out-of-range:** removal of unphysical values (e.g. negative shortwave radiation) using the ALMA expected range protocol (Bowling and Polcher, 2001).
2. **Night:** nocturnal shortwave radiation set to zero, based on civil twilight (when the sun is 6° below the horizon (Forsythe et al., 1995)).
3. **Constant:** four or more timesteps with identical values (excluding zero values for shortwave radiation, rainfall and snowfall) are removed as suspicious.
4. **Outlier:** values outside ± 4 standard deviations for each hour in a rolling 30-day window (to account for diurnal and seasonal variations) removed. Repeat with a larger tolerance (± 5 standard deviations) until no outliers remain (Schmid et al., 2000). The outlier test is not applied to precipitation.
5. **Visual:** remaining suspect readings are removed manually via visual inspection.

These steps are undertaken in the processing script *qc_observations.py* (see Sect 5: *Code availability*), including periods identified through visual inspection (21 instances across all data). Data removed through quality control are indicated in plots of each variable at each site included in the data collection (Lipson et al., 2022). Unaltered (raw) data are also included in the collection.

Communication, or human errors, also have the potential to degrade or invalidate data (Menard et al., 2021). As part of quality assurance, project coordinators prepared an observational data protocol (Lipson et al., 2021) to explicitly set out requirements for data providers prior to submission of their data. The protocol documented instrument siting requirements, variables and data formats, dataset length and resolution, necessary site characteristic information and metadata, as well as the expectations for data handling, use and authorship. On receiving data, coordinators undertook further checks and identified errors that were not be picked up by automated quality control. Identified errors included mislabelled variables and metadata, inconsistent timestamps and unit discrepancies. Many of the errors were identified by comparing provided data with secondary sources such as ERA5, nearby meteorological stations or previous publications. Errors were corrected collaboratively with data providers, some leading to corrections in primary data sources.

2.4 Gap-filling

Three gap filling methods are used to create a continuous dataset for forcing variables, in this order:

- contemporaneous and nearby flux tower or weather observing sites (where available from data providers)
- small gaps (≤ 2 hours) are linearly interpolated from the adjoining observations
- larger gaps and a 10-year spin-up period are filled with bias corrected ERA5 data (Section 2.6).

As only one site provided observed snowfall rate (JP-Yoyogi), ERA5 snowfall rates are used for all periods at other sites. At those sites the additional water equivalent from ERA5 snowfall is removed from subsequent observed rainfall until mass balance of observed total precipitation is achieved. This corrects melting snow being recorded as rainfall.



2.5 ERA5 reanalysis data

200 The ERA5 reanalysis product (Hersbach et al., 2020) assimilates global satellite, atmospheric and ground-based observations to constrain numerical weather prediction simulations, producing global output at 0.25° spatial and hourly temporal resolutions from 1979 to the present. It is therefore useful as a globally consistent and accessible source of meteorological data across space and time. ERA5, and its lower resolution predecessor ERA-Interim (Dee et al., 2011), have been used extensively to provide meteorological forcing data to drive land surface models and gap fill flux tower observations (Vuichard and Papale, 2015; Kokkonen et al., 2018; Pastorello et al., 2020; Ukkola et al., 2017, 2022).

205 The ERA5 hourly single level (Hersbach et al., 2018) dataset (retrieved from NCI Australia (Druken, 2020)) is used for gap-filling missing observations within the focus periods (Table 1) and for the 10-year model spin-up period. However, combining ERA5 data directly with urban flux tower observations has several deficiencies.

Grid-scale ERA5 data are not directly compatible with point-scale urban flux tower observations. This incompatibility is three-fold:

- 210 1. **Horizontally:** The ERA5 grid cell area (of order $30 \times 30 \text{ km}^2$) does not match the flux footprint from tower observations (of order 1 km^2). The ERA5 surface characteristics, including elevation, are based on an average description for the grid which may differ from surface characteristics around the observing tower, particularly in coastal or mountainous regions (Martens et al., 2020) in which many cities are located.
- 215 2. **Vertically:** ERA5 provide near-surface variables (2 or 10 m above ground level), aligning with World Meteorological Organization (WMO) guidelines for standard regional observations taken over short grass (World Meteorological Organization, 2008). As the urban roughness elements (e.g. buildings) are much taller than grass, instruments are mounted on towers at heights greater than 2 – 5 times average building height in order to be located within the inertial sub layer or constant flux layer (Velasco and Roth, 2010; Barlow, 2014; Grimmond and Ward, 2021).
- 220 3. **Land surface:** As the current operational ERA5 modelling systems do not include an urban land surface scheme (Boussetta et al., 2013; McNorton et al., 2021), other land types (grass, crops, shrubs, trees etc.) are to characterise the grid cell (Table 4). Urban land surfaces are well known to alter local meteorological conditions (Oke et al., 2017), therefore ERA5 output will likely differ from locally observed conditions.

225 Outside of cities there are known diurnal and seasonal biases between the ERA5 near-surface variables and observations (Haiden et al., 2018; Betts et al., 2019; Nogueira, 2020; Martens et al., 2020; Jiang et al., 2021). These biases are an outcome of simplifying assumptions made in model parameterisations and inadequacies of modelling frameworks in general (Cucchi et al., 2020). Various approaches to reduce ERA5 biases in non-urban areas have been proposed. For example, the Water and Global Change (WATCH) Forcing Data (WFD) project use gridded observations to bias-correct ERA-Interim data (Weedon et al., 2011), and more recently ERA5 data, creating the global WFDE5 dataset for impact studies (Cucchi et al., 2020). WFDE5



230 relies on the Climate Research Unit (CRU) monthly timeseries of gridded observations with resolution coarser than ERA5
 (New et al., 1999), requiring ERA5 to be regridded to a lower resolution. This may reduce the representativeness of the ERA5
 data, particularly in heterogeneous or complex terrain.

Alternatively, local observations can be used to bias-correct ERA data, e.g. the linear regression corrections using tower
 observations applied to FLUXNET datasets (Vuichard and Papale, 2015; Pastorello et al., 2020). However, linear methods
 235 neither conserve the variability of observations (Vuichard and Papale, 2015) (Section 3), nor can they correct diurnal timing
 differences within ERA5 data (e.g. out of phase from urban temporal profiles, which are typically delayed compared with non-
 urban surfaces used in ERA5, Figure 4, Table 4).

To account for these deficiencies, we develop a novel set of methods to bias correct ERA5 data to better represent observed
 urban conditions (Section 2.6).

240 **Table 4:** ERA5 surface cover information for grid cells in which the urban flux towers are located (Table 1). The land surface model used
 for ERA5 simulations does not account for urbanised land surfaces, nor vegetation types typical at urban sites. ERA5 surface roughness
 values are indicative as they vary slightly through time. Effective roughness is a correction accounting for observed urban mean wind speeds.

Site	ERA5 low vegetation	ERA5 high vegetation	low vegetation fraction	high vegetation fraction	lake (or sea) fraction	bare soil fraction	ERA5 surface roughness [m]	effective roughness [m]
AU-Preston	tall grass	interrupted forest	0.484	0.407	0.088	0.021	0.514	0.289
AU-SurreyHills	tall grass	interrupted forest	0.484	0.407	0.088	0.021	0.514	0.368
CA-Sunset	crops, mixed farming	evergreen needleleaf trees	0.205	0.723	0.071	0.000	1.077	1.508
FI-Kumpula	crops, mixed farming	evergreen needleleaf trees	0.296	0.352	0.137	0.215	0.708	0.703
FI-Torni	crops, mixed farming	evergreen needleleaf trees	0.296	0.352	0.137	0.215	0.708	0.424
FR-Capitole	crops, mixed farming	interrupted forest	0.920	0.050	0.004	0.025	0.291	0.519
GR-HECKOR	crops, mixed farming	interrupted forest	0.172	0.463	0.158	0.207	0.505	1.187
JP-Yoyogi	semidesert	no vegetation recorded	0.943	0.000	0.010	0.047	0.015	0.649
KR-Jungnang	crops, mixed farming	evergreen needleleaf trees	0.781	0.168	0.051	0.000	0.516	0.074
KR-Ochang	irrigated crops	interrupted forest	0.281	0.716	0.003	0.000	0.844	0.181
MX-Escandon	evergreen shrubs	mixed forest/woodland	0.743	0.216	0.006	0.035	0.404	0.229
NL-Amsterdam	crops, mixed farming	interrupted forest	0.867	0.061	0.056	0.015	0.248	0.254
PL-Lipowa	crops, mixed farming	interrupted forest	0.855	0.144	0.001	0.000	0.250	0.306
PL-Narutowicza	crops, mixed farming	interrupted forest	0.855	0.144	0.001	0.000	0.250	0.558
SG-TelokKurau06	irrigated crops	interrupted forest	0.905	0.021	0.074	0.000	0.335	0.309
UK-KingsCollege	crops, mixed farming	interrupted forest	0.609	0.372	0.020	0.000	0.504	0.315
UK-Swindon	crops, mixed farming	interrupted forest	0.727	0.251	0.001	0.021	0.397	0.146
US-Baltimore	crops, mixed farming	deciduous broadleaf trees	0.044	0.908	0.048	0.000	1.675	1.076
US-Minneapolis1	crops, mixed farming	interrupted forest	0.228	0.706	0.059	0.006	0.814	0.242
US-Minneapolis2	crops, mixed farming	interrupted forest	0.228	0.706	0.059	0.006	0.814	0.406
US-WestPhoenix	semidesert	evergreen needleleaf trees	0.949	0.051	0.000	0.000	0.084	0.404

2.6 Bias-correction methods

Bias-correction approaches used in the collection depend on the forcing variable (Table 2) and are described below.



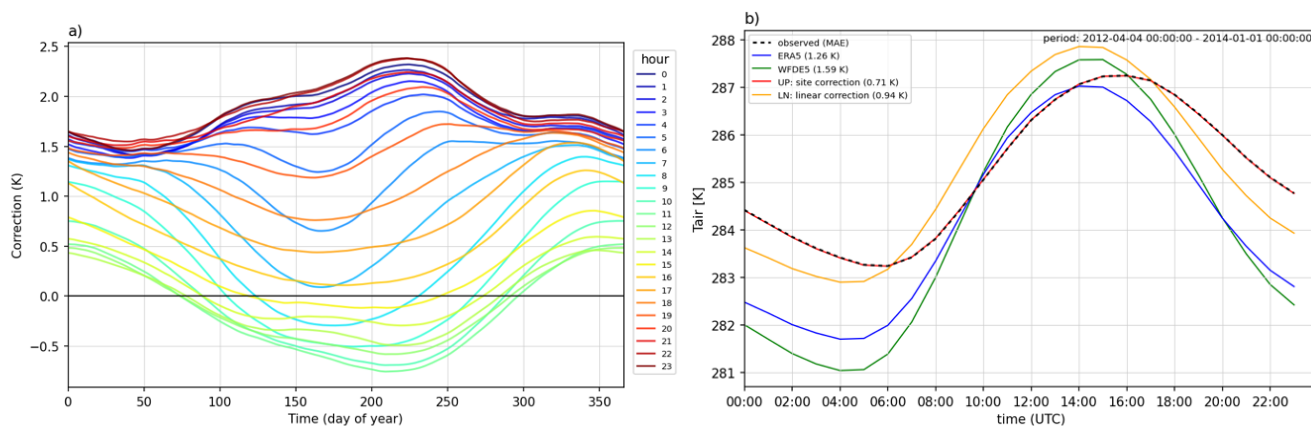
2.6.1 Hourly and daily corrections

245 For incoming longwave radiation, air temperature, specific humidity and air pressure, the mean bias between ERA5 and local flux tower observations are calculated for each hour (h) and each day of a year (D) in a 60-day rolling window of a representative year (Fig. 4a). The calculated bias $\eta_{bias}(D, h)$ is subtracted from the complete ERA5 timeseries $\eta_{ERA5}(t)$ to create a new corrected timeseries:

$$\eta(t) = \eta_{ERA5}(t) - \eta_{bias}(D, h). \quad (1)$$

250 The ERA5 data is from the grid nearest the observation site with at least 50% land. The resulting corrected timeseries (e.g. Fig. 4b) is used for gap filling site observations and for the spin up period. The subroutine *rolling_hourly_bias_correction* in the file *pipeline_functions.py* (Section 5) undertakes corrections with the following steps:

1. If observations have a 30-min resolution, average to 60-min to match ERA5 periods
2. Remove ERA5 data for time periods where site observations are missing
- 255 3. Calculate mean for each hour with both data sets to create a ‘representative’ year of 366 days
4. Extend to a three-year period by duplication to provide smoother transitions at year end
5. Calculate hourly means in a 60-day rolling window across the repeating timeseries, excluding data in windows with less than 30 observations. Repeat mean calculation for greater smoothing.
6. Calculate a timeseries of the bias between observed and ERA5 rolling means
- 260 7. Fill gaps in the bias timeseries by linear interpolation through each hour separately
8. Remove first and last year in the bias timeseries, using only the central year to bias correct each hour in the original ERA5 timeseries



265 **Figure 4:** Urban-PLUMBER reanalysis bias correction methods. Demonstrated using air temperature (T_{air}) for the grid containing the King’s College London site (UK-KingsCollege). (a) hourly (colour) bias calculated for each day of a ‘representative’ year and applied to entire ERA5 timeseries; (b) diurnal hourly mean Urban-PLUMBER correction (UP, red), observations (black), original ERA5 data (blue),



WFDE5 bias corrected data (green) and linear bias correction method used in FLUXNET (LN, yellow). Our new UP method has smaller mean absolute errors (MAE) overall, and can correct both pattern and phase errors of ERA5 (Section 3).

2.6.2 Logarithmic wind profile correction

270 Wind speed differences between ERA5 and site observations can result from errors in modelled synoptic-scale speeds, differences in representative heights, and differences in surface aerodynamic properties like roughness and displacement height. To correct bias and maintain standard deviations of the wind components (U,V) of observations at sensor height (z_{site}), the following correction to ERA5 data is undertaken assuming both a logarithmic wind profile and neutral conditions (Goret et al., 2019):

$$275 \quad u_{corr} = u_{ERA5} \frac{\ln\left(\frac{z_{site}-d_{site}}{z_{0,site}}\right)}{\ln\left(\frac{z_{grid}-d_{grid}}{z_{0,grid}}\right)}, \quad (2)$$

where u_{corr} is the corrected wind speed at z_{site} . The ERA5 wind (u_{ERA5}) at 10 m (z_{grid}) is used with the site surface roughness ($z_{0,site}$) and displacement height (d_{site}), grid roughness ($z_{0,grid}$) (Table 4) while assuming grid displacement height (d_{grid}) is zero for simplicity. If the resulting mean value of u_{corr} differs from observed mean value by more than 0.01 m s^{-1} , then $z_{0,grid}$ is iteratively adapted until this threshold accuracy in mean wind speed is achieved. Derived $z_{0,grid}$ values are given in Table
280 4 (last column). Note this approach ignores seasonal effects from vegetation phenology and directional effects but ensures mean wind speeds are appropriate at the urban z_{site} while conserving variability within the ERA5 derived wind data.

2.6.3 Long term precipitation correction

Total precipitation is an important variable in urban land surface models because of the effect on soil moisture which evolves over multi-year periods (Best and Grimmond, 2014). Most of the observational datasets included are not long enough to capture
285 interannual variations. We therefore use longer term total precipitation (P) from nearby stations from the Global Historical Climatology Network - Daily (GHCND) (Menne et al., 2012) over a 10 year period to correct ERA5 rain and snow fluxes (ϕ) at each timestep:

$$\phi_{corr} = \frac{\sum_{i=1}^{10 \text{ yrs}} P_{GHCND}}{\sum_{i=1}^{10 \text{ yrs}} P_{ERA5}} \phi_{ERA5}(t). \quad (3)$$

Gaps in the nearest GHCND station data are progressively filled by the next nearest station until no gaps are present. If gaps
290 could not be filled with GHNCN stations within 2° of latitude and longitude from the flux tower, and no alternative records are found (e.g. from national meteorological and hydrological services), then ERA5 rates are used unadjusted (*viz.*, KR-Ochang and KR-Jungnang). This assumes precipitation occurs on the same dates and at the same times in ERA5 and observed datasets, which may become less valid under increasingly convective conditions.



2.6.4 Linear bias correction

295 The FLUXNET2015 collection of 212 flux tower sites (Pastorello et al., 2020) bias correction method uses linear regression between site observations and reanalysis data to derive one slope (s) and intercept (b) per site, hence ‘unbiasing’ all ERA timesteps (i) :

$$LN_i = s \cdot ERA5_i + b. \quad (4)$$

Following FLUXNET2015, global radiation and wind fields are assigned an intercept of zero, and precipitation is not linearly modified (Vuichard and Papale, 2015). FLUXNET2015 use the coarser resolution ERA-Interim (spatial: 0.5° cf. 0.25° ; 300 temporal 3-h cf. 1-h) than ERA5. In this evaluation we use ERA5, which is found to be a consistent improvement over ERA-Interim (Albergel et al., 2018). However, after assessment we chose not to use a linear method (LN) for correcting variables in this collection. Its description is retained here for comparison purposes (Section 3).

3 Gap-filling evaluation

305 Site observations are quality controlled by individual data providers and collectively for this project (Section 2.3). The observed data required for forcing land surface models are then gap filled using a novel method of bias correcting reanalysis data. In this section, four methods which draw on ERA5 data are evaluated:

1. **ERA5**: nearest land based 0.25° resolution ERA5 (Hersbach et al., 2018, p.5) grid without bias correction
2. **W5**: nearest WFDE5 (Cucchi et al., 2020, p.5) grid (which uses bias correction from 0.5° CRU monthly gridded observations)
3. **UP**: the Urban-PLUMBER methods described here (using site observations for bias correction)
4. **LN**: linear methods based on FLUXNET2015 (Vuichard and Papale, 2015; Pastorello et al., 2020) (using site observations for bias correction)

To evaluate the methods available for gap filling, quality-controlled tower site observations (O_i) are used to assess the 315 calculated value (η) at timestep i using three metrics:

- a) Mean bias error (MBE): $\frac{\sum_{i=1}^n \eta_i - O_i}{n}$
- b) Mean absolute error (MAE): $\frac{\sum_{i=1}^n |\eta_i - O_i|}{n}$
- c) Normalised standard deviation (nSD): $\frac{\sum_{i=1}^n (\eta_i - \bar{\eta})^2}{n-1} \bigg/ \frac{\sum_{i=1}^n (O_i - \bar{O})^2}{n-1}$

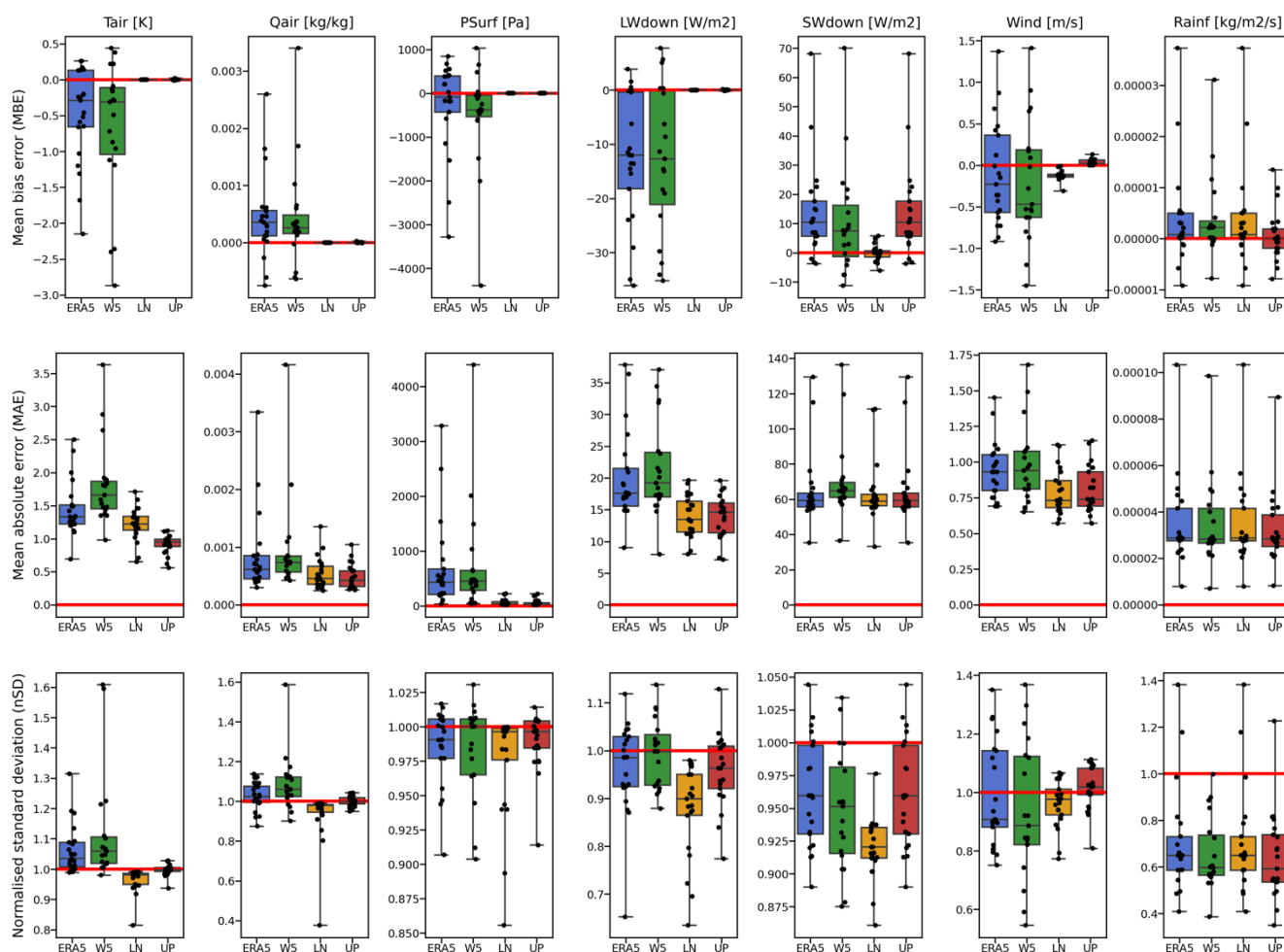
where \bar{O} and $\bar{\eta}$ are time-averaged over n data points. The time stamps for each variable are made consistent between the data 320 sources: ERA5 are hourly time ending data (Hersbach et al., 2018, p.5); 60-min site observations are hour ending; 30-min site



observations are converted to 60-min time ending by averaging; whereas as the WFDE5 SWdown, LWdown and Rainf are natively 60-min time beginning (Cucchi et al., 2020, p.5) they are shifted forward to match the time ending timestamps; and WFDE5 Tair, Qair, Psurf and Wind are instantaneous samples on the hour so their time stamp remains unchanged.

To summarise each metric for the 20 sites, we use boxplots (Fig. 5) for the seven forcing variables. The evaluation inherently
325 considers the net differences associated with both the spatial (vertical and surface cover) differences and errors (model and observation) from the two datasets. Uncorrected ERA5 (blue, Fig. 5) biases are generally negative for Tair, LWdown and Wind, and generally positive for Qair and SWdown. These biases can be partly explained by the ERA5 framework not including an urban surface model. For example, the well-documented warmer air temperature in cities (urban heat island) are not modelled in ERA5 because natural land surfaces are assumed in simulations (Table 4), although ERA5 can include an
330 urban signal if the data assimilated are from within urban areas (Tang et al., 2021). Qair shows a general positive bias as evapotranspiration will be overestimated in ERA5 without an urban land surface representation. Likewise, ERA5 SWdown are overestimated and LWdown underestimated possibly because urban air pollution effects are not included (Oke, 1988).

Other discrepancies between ERA5 data and site data arise from elevation differences in height above sea level (asl) of the ERA5 grid and site. For example, the MX-Escandon tower in Mexico City measurement height is 2277 m asl, whereas the
335 ERA5 grid cell is assigned a surface elevation of 2540 m asl because the cell includes nearby mountains. This 263 m difference causes a negative bias to Psurf of 2594 Pa and contributes to a Tair difference of -2.15 K. Additionally, orographic uplift increases the grid cell rainfall, leading to positive ERA5 bias of $2.25 \times 10^{-5} \text{ kg m}^{-2} \text{ s}^{-1}$ (+710 mm year⁻¹) compared with the MX-Escandon site observations. The ERA5 rainfall bias is even more pronounced at CA-Sunset in Vancouver, Canada, with a +1178 mm year⁻¹ bias. These results are consistent with other studies highlighting discrepancies between reanalysis and local
340 data in mountainous regions (Kokkonen et al., 2018).



345 **Figure 5:** Evaluation of bias correction methods. Four methods (colour) to create gap filled observed time series data: ERA5 (blue), WFDE5 (W5, green), linear debiasing (LN, orange), UP (red, this study) using (row 1) mean bias error, (row 2) mean absolute error, (row 3) normalised standard deviation, with the 20 individual sites (dots), and ideal agreement with observations (red line) and boxplot showing distribution. The UP corrections (selected for use in this study) have lower overall errors (cf. other methods) except SWdown, where no corrections to ERA5 are applied.

4 Data records

350 4.1 Data format

Timeseries data and site descriptive metadata are recorded in both plain text and netCDF4 (Rew et al., 1989) formats. Each site folder contains the following timeseries:

- [sitename]_raw_observations_[version]: site observed before project-wide quality control and gap filling (Table 1 gives period)



- 355
- [sitename]_clean_observations_[version]: after project-wide quality control and gap filling (Table 1 gives period)
 - [sitename]_metforcing_[version]: continuous observations with reanalysis-derived data after quality control and gap filling (Table 2; forcing data for 10-year spin up, then Table 1 periods)
 - [sitename]_era5_corrected_[version]: continuous timeseries (1990-2020) of bias corrected ERA5 reanalysis meteorological data (as used for gap filling and prepending metforcing observations)
- 360 Each site folder also contains the following site metadata:
- [sitename]_sitedata_[version].csv: comma separated text file for site characteristics metadata e.g. latitude, longitude, surface cover fraction, morphology etc. (Table 5, 6). This site characteristic data is also included within the metforcing netcdf (for convenience)
 - index.html: A summary page of site information in html format, including site characteristics, site images, timeseries, gap filling, quality control and diurnal plots
- 365

4.2 Timeseries metadata

The timeseries files include the following metadata:

- **title**: short description of the file
- **summary**: longer description of the file
- 370 • **sitename**: site code (e.g. AU-Preston)
- **long_sitename**: site long name, including city and country information
- **version**: version of current file
- **time_coverage_start**: start of timeseries in UTC (includes spin-up)
- **time_coverage_end**: end of timeseries in UTC
- 375 • **time_analysis_start**: start of observed (focus) period in UTC
- **time_shown_in**: time standard (always UTC)
- **local_utc_offset_hours**: offset in hours of local time from UTC
- **timestep_interval_seconds**: period of block averaging in seconds (timestep)
- **timestep_number_spinup**: number of timesteps prior to observed focus period
- 380 • **timestep_number_analysis**: number of timesteps in observed focus period
- **project_contact**: contact details for the Urban-PLUMBER project coordinators
- **observations_contact**: contact details of the observational site data providers
- **observations_reference**: published references associated with the observations
- **date_created**: date and time of creation of this file



- 385
- **source:** repository for processing code
 - **comment:** additional comments associated with this dataset (e.g. excluded wind sectors).

The netCDF files also include the following metadata for each variable

- **long_name:** plain language description of variable
- **standard_name:** equivalent variable name under the CF (climate and forecast) conventions
- 390 • **units:** SI (international system) units
- **ancillary_variables:** name of the associated quality control flag variable

NetCDF files also include site characteristics parameter values and descriptions (Table 5). Note, the `local_utc_offset` does not account for day light savings. As the onset/finishing of day light savings causes distinct behaviour changes it is critical users of the data consider this in their applications.

395 4.3 Site characteristics metadata

Site characteristics (Table 5, 6) are essential for any use of these data, and fundamental to application of land surface models. These metadata are provided in two machine readable forms (plain text in csv files, and netCDF4). The metadata are primarily drawn from published sources, or as advised by the data providers. If local parameters are not known values are estimated from high resolution global datasets or derived from empirical relations. The sources for each parameter are included within
400 the site characteristic metadata.

There are numerous methods to estimate the probable extent and weighting of turbulent fluxes footprints relative to the eddy covariance sensors located on a flux tower (Velasco and Roth, 2010). The eddy covariance flux footprint provides a basis to identify which area (and weighting) should be used to estimate the land surface fractions impacting the measurements. Some studies in this collection determine the footprint and resulting land cover fractions dynamically (e.g. for each 30-min period),
405 whereas others assumed a constant radius (e.g. based on a climatological analysis or rule of thumb) (Table 6). Standardising the method to determine land cover fractions across sites is beyond the scope of this work, so users of metadata should be mindful of these differences.

Different methods for estimating surface roughness length and zero-plane displacement height can give significantly different values (Kent et al., 2017). Given different sites have derived values using different methods we also provide values using two
410 consistent morphometric methods (Macdonald (Macdonald et al., 1998) and Kanda (Kanda et al., 2013); Table 5, parameters 26 – 29) derived from surface fraction and building height parameters within the measurement footprint (Table 6). The Kanda modification to the Macdonald method accounts for the variability in roughness element height, resulting in larger displacement heights which are closer to estimates made with anemometric methods (Kent et al., 2017). The Macdonald method assumes that all the buildings have the same average roughness element height. However, care must be taken when using



415 Kanda values as some urban land surface models expect displacement height to be always lower than average building height (Hertwig et al., 2020).

Where not known, building height standard deviation (σ_H) is estimated from an empirical relation to building mean height (H_{ave}) (Kanda et al., 2013):

$$\sigma_H = 1.05H_{ave} - 3.7. \quad (5)$$

420 Similarly, unknown local wall to plan area ratios (λ_w) are derived from roof area fraction (λ_p) and canyon height to width ratio (H/W) assuming an infinite canyon geometry (Masson et al., 2020):

$$\lambda_w = 2(1 - \lambda_p)H/W. \quad (6)$$

Frontal area index (λ_f) is sometimes reported in site literature without H/W or λ_w , in which case these are estimated (again assuming an infinite canyon geometry) with (Porson et al., 2010):

425
$$\lambda_f = \frac{2}{\pi}(1 - \lambda_p)H/W. \quad (7)$$

Where not known or provided, mean annual anthropogenic heat flux (Varquez et al., 2021) or soil characteristics (Hengl, 2018a, b, c) are estimated from global datasets at 1 km or lower resolutions.

Table 5: Site characteristic metadata description and units. Select values are provided in Table 6.

ID	Parameter	Units	Description
1	latitude	degrees_north	Latitude of tower
2	longitude	degrees_east	Longitude of tower
3	ground_height	m	Height above sea level of base of tower
4	measurement_height_above_ground	m	Height above ground level (agl) of eddy covariance equipment on tower
5	impervious_area_fraction	1	Plan area fraction of all impervious (hard) surfaces, including roofs, roads, paths and paved areas
6	tree_area_fraction	1	Plan area fraction of tree canopy (> 2 m)
7	grass_area_fraction	1	Plan area fraction of grass or other vegetation (< 2 m)
8	bare_soil_area_fraction	1	Plan area fraction of bare soil
9	water_area_fraction	1	Plan area fraction of water
10	roof_area_fraction	1	Plan area fraction of roofs (λ_p)
11	road_area_fraction	1	Plan area fraction of roads
12	other_paved_area_fraction	1	Plan area fraction of hard surfaces on ground excluding roads (e.g. paths, plazas, carparks etc)
13	building_mean_height	m	Mean height above ground of buildings (H_{ave})
14	tree_mean_height	m	Mean height above ground of trees
15	roughness_length_momentum	m	Aerodynamic roughness length for momentum as reported in literature or provided by data providers
16	displacement_height	m	Zero-plane displacement height as reported in literature or advised by data providers
17	canyon_height_width_ratio	1	Mean building height to mean street canyon width (distance between buildings) ratio (H/W)



ID	Parameter	Units	Description
18	wall_to_plan_area_ratio	1	Sum of wall surface area to plan area ratio (λ_w)
19	average_albedo_at_midday	1	Median site albedo at midday (local standard time) for available observations
20	resident_population_density	person km ⁻²	Resident (night) population density
21	anthropogenic_heat_flux_mean	W m ⁻²	Anthropogenic heat flux annual mean
22	topsoil_clay_fraction	1	Clay fraction of topsoil
23	topsoil_sand_fraction	1	Sand fraction of topsoil
24	topsoil_bulk_density	kg m ⁻³	Bulk (dry) density of topsoil
25	building_height_standard_deviation	m	standard deviation of building heights (σ_H)
26	roughness_length_momentum_mac	m	Aerodynamic roughness length for momentum calculated by the Macdonald morphometric method
27	displacement_height_mac	m	Zero-plane displacement height calculated by the Macdonald morphometric method
28	roughness_length_momentum_kanda	m	Aerodynamic roughness length for momentum calculated by the Kanda morphometric method
29	displacement_height_kanda	m	Zero-plane displacement height calculated by the Kanda morphometric method

430 **Table 6:** Select site characteristic values (see Table 5 for definitions). Other site characteristic values and sources are provided within the collection (Lipson et al., 2022). Areas analysed for land cover fractions and roughness parameters are based on either a static radius around the flux tower (value given) or a dynamic footprint model (fpm), depending on the available site literature.

Parameter	surface cover fraction assumption	ground_height	measurement_height_above_ground	impervious_area_fraction	tree_area_fraction	grass_area_fraction	bare_soil_area_fraction	water_area_fraction	roof_area_fraction	road_area_fraction	other_paved_area_fraction	building_mean_height
AU-Preston	500m	93	40	0.620	0.225	0.150	0.005	0	0.445	0.130	0.045	6.4
AU-SurreyHills	500m	97	38	0.54	0.29	0.15	0.01	0.01	0.39	0.09	0.06	7.2
CA-Sunset	fpm	78	24.8	0.68	0.12	0.20	0	0	0.23	0.20	0.25	4.9
FI-Kumpula	1000m	29	31	0.46	0.30	0.24	0	0	0.14	0.32	0	12.6
FI-Torni	1000m	15.2	60	0.77	0.15	0.07	0	0.01	0.37	0.25	0.15	17.9
FR-Capitole	500m	143	48.05	0.90	0.08	0.02	0	0	0.62	0.28	0	15
GR-HECKOR	fpm	30	27	0.916	0.040	0.016	0.010	0.019	0.516	0.201	0.199	11.3
JP-Yoyogi	500m	39	52	0.92	0.06	0.01	0.01	0	0.41	0.32	0.19	9.0
KR-Jungnang	500m	22	41.5	0.965	0	0.019	0.016	0	0.588	0.377	0	8.648
KR-Ochang	500m	60	19	0.470	0.184	0.333	0.013	0	0.133	0.337	0	7.384
MX-Escandon	fpm	2240	37	0.94	0.06	0	0	0	0.57	0.37	0	9.69
NL-Amsterdam	500m	0	40	0.68	0.15	0	0	0.17	0.44	0.07	0.17	14.2
PL-Lipowa	fpm	204	37	0.76	0.16	0.08	0	0	0.35	0.21	0.20	10.2
PL-Narutowicza	500m	221	42	0.65	0.22	0.09	0.04	0	0.29	0.19	0.17	16



SG-TelokKurau06	1000m	5	20.7	0.85	0.11	0.04	0	0	0.39	0.12	0.34	9.9
UK-KingsCollege	fpm	14.5	50.3	0.79	0.03	0.04	0	0.14	0.40	0.39	0	21.3
UK-Swindon	500m	108	12.5	0.49	0.09	0.36	0.06	0	0.16	0.15	0.18	4.5
US-Baltimore	1000m	157	37.2	0.313	0.536	0.138	0.007	0.006	0.160	0.153	0	5.6
US-Minneapolis1	fpm	301	40	0.21	0.38	0.36	0	0.05	0.12	0.05	0.04	5.05
US-Minneapolis2	fpm	301	40	0.05	0.2	0.73	0	0.02	0.01	0	0.04	5.05
US-WestPhoenix	fpm	340	22.1	0.48	0.05	0.10	0.37	0	0.26	0.22	0	4.5

4.4 Data flags

Each variable for each timestep has a quality control (qc) flag. For example, LWdown_qc lists qc flags for LWdown at each
 435 timestep. Flag numbers are consistent across all variables:

0. observed by measurement at site and passes project quality control tests
1. filled by observation: interpolated from site observations over short (2 h) periods OR filled by observations from nearby (< 10 km) stations over longer periods
2. filled by ERA5: derived from ERA5 with site specific bias correction
- 440 3. missing or removed through quality control (occurs only in timeseries without gap filling)

4.5 Wind sector exclusions

Turbulent flux data are excluded from certain wind directions (Table 7) because of:

- interference on flow from tower structure (as identified by data providers)
- markedly different land cover characteristics from sectors of interest (with guidance from data providers)

445 The US-Minneapolis site has different surface cover by wind direction but is retained in the collection because of its both a long observation period and its distinct land cover characteristics. Following previous studies (Menzer and McFadden, 2017) we subdivide this data into low-density residential area (northern sectors, US-Minneapolis2) and irrigated grassland with few built structures (south, US-Minneapolis1). Each are given their own site timeseries and metadata, resulting in 21 datasets.

Table 7: Site wind sector exclusions. Sites with sensible and latent heat fluxes excluded because of land cover or land use
 450 differences by wind sectors as described in the reference provided. Maps of these sectors are provided in the site data collection(Lipson et al., 2022).

Sitename	Sectors excluded	Reason	Reference
FI-Kumpula	0-180°, 320-360°	surface inhomogeneity	(Karsisto et al., 2016)
FI-Torni	40-150°	flow interference from tower	(Järvi et al., 2018)
JP-Yoyogi	170-260°	surface inhomogeneity	(Ishidoya et al., 2020)
US-Minneapolis1	75-285°	surface inhomogeneity	(Menzer and McFadden, 2017)
US-Minneapolis2	0-180°, 270-360°	120-180°: flow interference from tower 270-360°, 0-120°: surface inhomogeneity	(Menzer and McFadden, 2017)



5 Data availability

All site observational and characteristics data are openly available from <https://doi.org/10.5281/zenodo.6590886> (Lipson et al., 2022) under a Creative Commons Attribution licence (CC-BY-4.0).

455 We recommend data users consult with site contributing authors and/or the coordination team early (i.e. planning stage) in projects that plan to use these data. Relevant contacts are included in site metadata.

6 Code Availability

Code used to process datasets are available at <https://doi.org/10.5281/zenodo.6590942> (Lipson, M., 2022a).

Code used to create manuscript figures are available at <https://doi.org/10.5281/zenodo.6590941> (Lipson, M., 2022b).

460 7 Acknowledgements

We would like to thank the vast number of people involved in day-to-day running of these sites that have been involved in instrument and tower installations (permitting, purchasing and site installation), routine (and unexpected event) maintenance, data collection, routine data processing and final data processing. We thank all those that have provided sites for the towers to be located and sometimes power and internet access. We acknowledge the essential funding for the instrumentation and other
465 infrastructure, for staff (administrative, technical and scientific) and students for these activities. We also thank those who offered data for use in this project which are not included at this time.

The project coordinating team are supported by UNSW Sydney and the Australian Research Council (ARC) Centre of Excellence for Climate System Science (grant CE110001028), University of Reading, the Met Office and ERC urbisphere 855005. Computation support from the ARC Centre of Excellence for Climate Extremes (grant CE170100023) and National
470 Computational Infrastructure (NCI) Australia. Contains modified Copernicus Climate Change Service Information. Site-affiliated acknowledgments are listed in Table 10.

Table 8: Funding acknowledgements for individual sites.

Site	Contributing author	Site funding acknowledgements
AU-Preston	Andrew Coutts, Nigel Tapper	-
AU-SurreyHills	Andrew Coutts, Nigel Tapper	-
CA-Sunset	Andreas Christen, Oliver Michels	Canadian Foundation for Climate and Atmospheric Sciences (CFCAS, Project "Environmental Prediction in Canadian Cities (EPICC)") and the Natural and Engineering Research Council of Canada (NSERC, RGPIN-03958, RGPAS-507854). Some instruments were supported by the Canada Foundation for Innovation (CFI, IF 2015, grant no. 33600) and BCKDF. We acknowledge the support of BC Hydro to operate the tower.
FI-Kumpula	Leena Järvi	ICOS Finland



FI-Torni	Leena Järvi	ICOS Finland
FR-Capitole	Valéry Masson	Météo-France and CNRS
GR-HECKOR	Nektarios Chrysoulakis	EU Horizon 2020 Research and Innovation Programme, under Grant Agreement No 870337 project CURE (http://cure-copernicus.eu)
JP-Yoyogi	Hirofumi Sugawara	Japan Society for the Promotion of Science KAKENHI grants (nos. 24241008, 15H02814, 18K01129, and 19H01975), and the Environment Research and Technology Development Fund (JPMEERF20191009) of the Environmental Restoration and Conservation Agency of Japan
KR-Jungnang	Jinkyu Hong, Sungsoo Jo, Yeon-Hee	Korea Meteorological Administration Research and Development Program "Development of Production Techniques on User-Customized Weather information" under Grant (KMA2018-00622) and National Research Foundation of Korea (NRF) grants funded by the Korean government (NRF-2018R1A5A1024958)
KR-Ochang	Jinkyu Hong, Je-Woo Hong, Keunmin Lee	Korea Meteorological Administration Research and Development Program under Grant KMI2021-01610
MX-Escandon	Erik Velasco	National Institute of Ecology and Climate Change (INECC) and the Mexico City's Secretariat for the (SEDEMA) through the Molina Center for Energy and the Environment (MCE2).
NL-Amsterdam	Bert Heusinkveld	Netherlands Organisation for Scientific Research (NWO) Project 864.14.007 and the Amsterdam Institute for Advanced Metropolitan Solutions (AMS) project VIR16002.
PL-Lipowa	Włodzimierz Pawlak, Krzysztof Fortuniak	-
PL-Narutowicza	Włodzimierz Pawlak, Krzysztof Fortuniak	-
SG-TelokKurai06	Matthias Roth	National University of Singapore (research grant R-109-000-091-112).
UK-KingsCollege	Simone Kotthaus, Sue Grimmond	EUfp7 Grant agreement no. 211345 (BRIDGE) and NERC ClearLo (NE/H003231/1), NERC ARSF (GB08/19), EPSRC (EP/I00159X/1, EP/I00159X/2) and KCL.
UK-Swindon	Helen Ward, Jonathan Evans, Sue Grimmond	NERC NE/H52479X/1
US-Baltimore	Sue Grimmond, Ben Crawford	National Science Foundation (BCS-0095284, DEB-9714835) and USDA Forest Service.
US-Minneapolis	Joseph McFadden	NASA Earth Science Division (NNG04GN80G)
US-WestPhoenix	Stevan Earl, Winston Chow	National Science Foundation (DEB-1832016) Central Arizona-Phoenix Long-Term Ecological Research Program (CAP LTER)

7 Author Contributions

M.L., S.G. and M.B. conceived and coordinated the project, and prepared the protocols for contributing authors. M.L. collated
 475 site datasets, wrote processing code, developed and undertook analysis of bias correction methods, prepared figures, prepared datasets and drafted the manuscript with guidance from S.G. and M.B. All other authors (listed alphabetically) collected primary data, prepared site information, processed datasets for inclusion in the collection and contributed to the manuscript. Table 8 lists contributing author site affiliation.

The authors declare that they have no conflict of interest.



480 References

- Albergel, C., Dutra, E., Munier, S., Calvet, J.-C., Munoz-Sabater, J., de Rosnay, P., and Balsamo, G.: ERA-5 and ERA-Interim driven ISBA land surface model simulations: which one performs better?, 22, 3515–3532, <https://doi.org/10.5194/hess-22-3515-2018>, 2018.
- Arnfield, A. J.: Two decades of urban climate research: a review of turbulence, exchanges of energy and water, and the urban heat island, 23, 1–26, <https://doi.org/10.1002/joc.859>, 2003.
- 485 Aubinet, M., Vesala, T., and Papale, D.: Eddy Covariance: A Practical Guide to Measurement and Data Analysis, Springer Science & Business Media, 451 pp., 2012.
- Baldocchi, D. D.: How eddy covariance flux measurements have contributed to our understanding of Global Change Biology, 26, 242–260, <https://doi.org/10.1111/gcb.14807>, 2020.
- 490 Barlow, J. F.: Progress in observing and modelling the urban boundary layer, *Urban Climate*, 10, Part 2, 216–240, <https://doi.org/10.1016/j.uclim.2014.03.011>, 2014.
- Beck, H. E., Zimmermann, N. E., McVicar, T. R., Vergopolan, N., Berg, A., and Wood, E. F.: Present and future Köppen-Geiger climate classification maps at 1-km resolution, 5, 180214, <https://doi.org/10.1038/sdata.2018.214>, 2018.
- Beringer, J., Hutley, L. B., McHugh, I., Arndt, S. K., Campbell, D., Cleugh, H. A., Cleverly, J., Resco de Dios, V., Eamus, D., Evans, B., Ewenz, C., Grace, P., Griebel, A., Haverd, V., Hinko-Najera, N., Huete, A., Isaac, P., Kanniah, K., Leuning, R., Liddell, M. J., Macfarlane, C., Meyer, W., Moore, C., Pendall, E., Phillips, A., Phillips, R. L., Prober, S. M., Restrepo-Coupe, N., Rutledge, S., Schroder, I., Silberstein, R., Southall, P., Yee, M. S., Tapper, N. J., van Gorsel, E., Voté, C., Walker, J., and Wardlaw, T.: An introduction to the Australian and New Zealand flux tower network – OzFlux, 13, 5895–5916, <https://doi.org/10.5194/bg-13-5895-2016>, 2016.
- Best, M. J. and Grimmond, C. S. B.: Importance of initial state and atmospheric conditions for urban land surface models’ performance, 10, 387–406, <https://doi.org/10.1016/j.uclim.2013.10.006>, 2014.
- 500 Best, M. J., Abramowitz, G., Johnson, H. R., Pitman, A. J., Balsamo, G., Boone, A., Cuntz, M., Decharme, B., Dirmeyer, P. A., Dong, J., Ek, M., Guo, Z., Haverd, V., Hurk, B. J. J. van den, Nearing, G. S., Pak, B., Peters-Lidard, C., Santanello, J. A., Stevens, L., and Vuichard, N.: The Plumbing of Land Surface Models: Benchmarking Model Performance, 16, 1425–1442, <https://doi.org/10.1175/JHM-D-14-0158.1>, 2015.
- Betts, A. K., Chan, D. Z., and Desjardins, R. L.: Near-Surface Biases in ERA5 Over the Canadian Prairies, *Front. Environ. Sci.*, 7, <https://doi.org/10.3389/fenvs.2019.00129>, 2019.
- 505 Bjorkegren, A. B., Grimmond, C. S. B., Kotthaus, S., and Malamud, B. D.: CO₂ emission estimation in the urban environment: Measurement of the CO₂ storage term, *Atmospheric Environment*, 122, 775–790, <https://doi.org/10.1016/j.atmosenv.2015.10.012>, 2015.
- Boussetta, S., Balsamo, G., Beljaars, A., Panareda, A.-A., Calvet, J.-C., Jacobs, C., Hurk, B. van den, Viterbo, P., Lafont, S., Dutra, E., Jarlan, L., Balzarolo, M., Papale, D., and Werf, G. van der: Natural land carbon dioxide exchanges in the ECMWF integrated forecasting system: Implementation and offline validation, 118, 5923–5946, <https://doi.org/10.1002/jgrd.50488>, 2013.
- 510 Bowling, L. and Polcher, J.: The ALMA data exchange convention, 2001.
- Center for International Earth Science Information Network - CIESIN - Columbia University, International Food Policy Research Institute - IFPRI, The World Bank, and Centro Internacional de Agricultura Tropical - CIAT: Global Rural-Urban Mapping Project, Version 1 (GRUMPv1): Settlement Points, Revision 01, NASA Socioeconomic Data and Applications Center (SEDAC), Palisades, NY, 2017.
- 515 Chow, W.: Eddy covariance data measured at the CAP LTER flux tower located in the west Phoenix, AZ neighborhood of Maryvale from 2011-12-16 through 2012-12-31, <https://doi.org/10.6073/PASTA/FED17D67583EDA16C439216CA40B0669>, 2017.
- Chow, W. T. L., Volo, T. J., Vivoni, E. R., Jenerette, G. D., and Ruddell, B. L.: Seasonal dynamics of a suburban energy balance in Phoenix, Arizona, 34, 3863–3880, <https://doi.org/10.1002/joc.3947>, 2014.
- Christen, A., Coops, N. C., Crawford, B. R., Kellett, R., Liss, K. N., Olchovski, I., Tooke, T. R., van der Laan, M., and Voogt, J. A.: Validation of modeled carbon-dioxide emissions from an urban neighborhood with direct eddy-covariance measurements, *Atmospheric Environment*, 45, 6057–6069, <https://doi.org/10.1016/j.atmosenv.2011.07.040>, 2011.
- 520 Coutts, A. M., Beringer, J., and Tapper, N. J.: Characteristics influencing the variability of urban CO₂ fluxes in Melbourne, Australia, *Atmospheric Environment*, 41, 51–62, <https://doi.org/10.1016/j.atmosenv.2006.08.030>, 2007a.
- Coutts, A. M., Beringer, J., and Tapper, N. J.: Impact of Increasing Urban Density on Local Climate: Spatial and Temporal Variations in the Surface Energy Balance in Melbourne, Australia, *J. Appl. Meteor. Climatol.*, 46, 477–493, <https://doi.org/10.1175/JAM2462.1>, 2007b.
- 525 Crawford, B. and Christen, A.: Spatial source attribution of measured urban eddy covariance CO₂ fluxes, *Theor Appl Climatol*, 119, 733–755, <https://doi.org/10.1007/s00704-014-1124-0>, 2015.
- Crawford, B., Grimmond, C. S. B., and Christen, A.: Five years of carbon dioxide fluxes measurements in a highly vegetated suburban area, *Atmospheric Environment*, 45, 896–905, <https://doi.org/10.1016/j.atmosenv.2010.11.017>, 2011.



- 530 Cucchi, M., Weedon, G. P., Amici, A., Bellouin, N., Lange, S., Schmied, H. M., Hersbach, H., and Buontempo, C.: WFDE5: bias adjusted ERA5 reanalysis data for impact studies, 1–32, <https://doi.org/10.5194/essd-2020-28>, 2020.
- Dee, D. P., Uppala, S. M., Simmons, A. J., Berrisford, P., Poli, P., Kobayashi, S., Andrae, U., Balmaseda, M. A., Balsamo, G., Bauer, P., Bechtold, P., Beljaars, A. C. M., van de Berg, L., Bidlot, J., Bormann, N., Delsol, C., Dragani, R., Fuentes, M., Geer, A. J., Haimberger, L., Healy, S. B., Hersbach, H., Hólm, E. V., Isaksen, I., Kållberg, P., Köhler, M., Matricardi, M., McNally, A. P., Monge-Sanz, B. M., Morcrette, J.-J., Park, B.-K., Peubey, C., de Rosnay, P., Tavolato, C., Thépaut, J.-N., and Vitart, F.: The ERA-Interim reanalysis: configuration and performance of the data assimilation system, *Quarterly Journal of the Royal Meteorological Society*, 137, 553–597, <https://doi.org/10.1002/qj.828>, 2011.
- 535 Dou, J., Grimmond, S., Cheng, Z., Miao, S., Feng, D., and Liao, M.: Summertime surface energy balance fluxes at two Beijing sites, 39, 2793–2810, <https://doi.org/10.1002/joc.5989>, 2019.
- Druken, K.: ERA5 Replicated Datasets, NCI Australia, <https://doi.org/10.25914/5F48874388857>, 2020.
- 540 Feigenwinter, C., Vogt, R., and Christen, A.: Eddy Covariance Measurements Over Urban Areas, in: *Eddy Covariance: A Practical Guide to Measurement and Data Analysis*, edited by: Aubinet, M., Vesala, T., and Papale, D., Springer Netherlands, Dordrecht, 377–397, https://doi.org/10.1007/978-94-007-2351-1_16, 2012.
- Ferreira, M. J., de Oliveira, A. P., and Soares, J.: Diurnal variation in stored energy flux in São Paulo city, Brazil, *Urban Climate*, 5, 36–51, <https://doi.org/10.1016/j.uclim.2013.06.001>, 2013.
- 545 Forsythe, W. C., Rykiel, E. J., Stahl, R. S., Wu, H., and Schoolfield, R. M.: A model comparison for daylength as a function of latitude and day of year, *Ecological Modelling*, 80, 87–95, [https://doi.org/10.1016/0304-3800\(94\)00034-F](https://doi.org/10.1016/0304-3800(94)00034-F), 1995.
- Fortuniak, K., Kłysik, K., and Siedlecki, M.: New measurements of the energy balance components in Łódź, in: *Preprints, sixth International Conference on Urban Climate: 12-16 June, 2006, Göteborg, Sweden, Sixth International Conference On Urban Climate, Göteborg, Sweden*, 64–67, 2006.
- Fortuniak, K., Pawlak, W., and Siedlecki, M.: Integral Turbulence Statistics Over a Central European City Centre, 146, 257–276, <https://doi.org/10.1007/s10546-012-9762-1>, 2013.
- 550 Goret, M., Masson, V., Schoetter, R., and Moine, M.-P.: Inclusion of CO₂ flux modelling in an urban canopy layer model and an evaluation over an old European city centre, *Atmospheric Environment: X*, 3, 100042, <https://doi.org/10.1016/j.aeaoa.2019.100042>, 2019.
- Grimmond, C. S. B.: Progress in measuring and observing the urban atmosphere, *Theor. Appl. Climatol.*, 84, 3–22, <https://doi.org/10.1007/s00704-005-0140-5>, 2006.
- 555 Grimmond, C. S. B. and Oke, T. R.: Heat Storage in Urban Areas: Local-Scale Observations and Evaluation of a Simple Model, *J. Appl. Meteor.*, 38, 922–940, [https://doi.org/10.1175/1520-0450\(1999\)038<0922:HSIUAL>2.0.CO;2](https://doi.org/10.1175/1520-0450(1999)038<0922:HSIUAL>2.0.CO;2), 1999.
- Grimmond, C. S. B., Blackett, M., Best, M. J., Barlow, J., Baik, J.-J., Belcher, S. E., Bohnenstengel, S. I., Calmet, I., Chen, F., Dandou, A., Fortuniak, K., Gouvea, M. L., Hamdi, R., Hendry, M., Kawai, T., Kawamoto, Y., Kondo, H., Krayenhoff, E. S., Lee, S.-H., and Loridan, T.: The International Urban Energy Balance Models Comparison Project: First Results from Phase 1, *Journal of Applied Meteorology & Climatology*, 49, 1268–1292, <https://doi.org/10.1175/2010JAMC2354.1>, 2010.
- 560 Grimmond, C. S. B., Blackett, M., Best, M. J., Baik, J.-J., Belcher, S. E., Beringer, J., Bohnenstengel, S. I., Calmet, I., Chen, F., Coutts, A., Dandou, A., Fortuniak, K., Gouvea, M. L., Hamdi, R., Hendry, M., Kanda, M., Kawai, T., Kawamoto, Y., Kondo, H., Krayenhoff, E. S., Lee, S.-H., Loridan, T., Martilli, A., Masson, V., Miao, S., Oleson, K., Ooka, R., Pigeon, G., Porson, A., Ryu, Y.-H., Salamanca, F., Steeneveld, G. J., Tombrou, M., Voogt, J. A., Young, D. T., and Zhang, N.: Initial results from Phase 2 of the international urban energy balance model comparison, 31, 244–272, <https://doi.org/10.1002/joc.2227>, 2011.
- 565 Grimmond, S. and Christen, A.: Flux measurements in urban ecosystems, 5, 1–8, 2012.
- Grimmond, S. and Ward, H. C.: *Urban Measurements and Their Interpretation*, in: *Springer Handbook of Atmospheric Measurements*, edited by: Foken, T., Springer International Publishing, Cham, 1407–1437, https://doi.org/10.1007/978-3-030-52171-4_52, 2021.
- Haiden, T., Sandu, I., Balsamo, G., Arduini, G., and Beljaars, A.: Addressing biases in near-surface forecasts, 157, 20–25, 2018.
- 570 Hengl, T.: Clay content in % (kg / kg) at 6 standard depths (0, 10, 30, 60, 100 and 200 cm) at 250 m resolution (v0.2), <https://doi.org/10.5281/ZENODO.2525663>, 2018a.
- Hengl, T.: Sand content in % (kg / kg) at 6 standard depths (0, 10, 30, 60, 100 and 200 cm) at 250 m resolution (v0.2), <https://doi.org/10.5281/ZENODO.2525662>, 2018b.
- Hengl, T.: Soil bulk density (fine earth) 10 x kg / m-cubic at 6 standard depths (0, 10, 30, 60, 100 and 200 cm) at 250 m resolution (v0.2), <https://doi.org/10.5281/ZENODO.2525665>, 2018c.
- 575 Hersbach, H., Bell, B., Berrisford, P., Biavati, G., Horányi, A., Muñoz Sabater, J., Nicolas, J., Peubey, C., Radu, R., Rozum, I., and others: ERA5 hourly data on single levels from 1979 to present, Copernicus Climate Change Service (C3S) Climate Data Store (CDS), 2018.
- Hersbach, H., Bell, B., Berrisford, P., Hirahara, S., Horányi, A., Muñoz-Sabater, J., Nicolas, J., Peubey, C., Radu, R., Schepers, D., Simmons, A., Soci, C., Abdalla, S., Abellan, X., Balsamo, G., Bechtold, P., Biavati, G., Bidlot, J., Bonavita, M., Chiara, G. D., Dahlgren, P., Dee, D., Diamantakis, M., Dragani, R., Flemming, J., Forbes, R., Fuentes, M., Geer, A., Haimberger, L., Healy, S., Hogan, R. J., Hólm, E., Janisková, M., Keeley, S., Laloyaux, P., Lopez, P.,



- 580 Lupu, C., Radnoti, G., Rosnay, P. de, Rozum, I., Vamborg, F., Villaume, S., and Thépaut, J.-N.: The ERA5 global reanalysis, 146, 1999–2049, <https://doi.org/10.1002/qj.3803>, 2020.
- Hertwig, D., Grimmond, S., Hendry, M. A., Saunders, B., Wang, Z., Jeoffrion, M., Vidale, P. L., McGuire, P. C., Bohnenstengel, S. I., Ward, H. C., and Kotthaus, S.: Urban signals in high-resolution weather and climate simulations: role of urban land-surface characterisation, *Theor Appl Climatol*, 142, 701–728, <https://doi.org/10.1007/s00704-020-03294-1>, 2020.
- 585 Hirano, T., Sugawara, H., Murayama, S., and Kondo, H.: Diurnal Variation of CO₂ Flux in an Urban Area of Tokyo, 11, 100–103, <https://doi.org/10.2151/sola.2015-024>, 2015.
- Hong, J., Lee, K., and Hong, J.-W.: Observational data of Ochang and Jungnang in Korea, 2020.
- Hong, J.-W., Hong, J., Chun, J., Lee, Y. H., Chang, L.-S., Lee, J.-B., Yi, K., Park, Y.-S., Byun, Y.-H., and Joo, S.: Comparative assessment of net CO₂ exchange across an urbanization gradient in Korea based on eddy covariance measurements, *Carbon Balance and Management*, 14, 13, <https://doi.org/10.1186/s13021-019-0128-6>, 2019.
- 590 Ishidoya, S., Sugawara, H., Terao, Y., Kaneyasu, N., Aoki, N., Tsuboi, K., and Kondo, H.: O₂ : CO₂ exchange ratio for net turbulent flux observed in an urban area of Tokyo, Japan, and its application to an evaluation of anthropogenic CO₂ emissions, 20, 5293–5308, <https://doi.org/10.5194/acp-20-5293-2020>, 2020.
- Järvi, L., Rannik, Ü., Kokkonen, T. V., Kurppa, M., Karppinen, A., Kouznetsov, R. D., Rantala, P., Vesala, T., and Wood, C. R.: Uncertainty of eddy covariance flux measurements over an urban area based on two towers, 11, 5421–5438, <https://doi.org/10.5194/amt-11-5421-2018>, 2018.
- Jiang, Q., Li, W., Fan, Z., He, X., Sun, W., Chen, S., Wen, J., Gao, J., and Wang, J.: Evaluation of the ERA5 reanalysis precipitation dataset over Chinese Mainland, *Journal of Hydrology*, 595, 125660, <https://doi.org/10.1016/j.jhydrol.2020.125660>, 2021.
- Jo, S., Hong, J.-W., and Hong, J.: The observational flux measurement data of suburban and low-residential areas in Korea (in preparation), n.d.
- 600 Kanda, M., Inagaki, A., Miyamoto, T., Gryschka, M., and Raasch, S.: A New Aerodynamic Parametrization for Real Urban Surfaces, *Boundary-Layer Meteorol*, 148, 357–377, <https://doi.org/10.1007/s10546-013-9818-x>, 2013.
- Karsisto, P., Fortelius, C., Demuzere, M., Grimmond, C. S. B., W., O. K., Kouznetsov, R., Masson, V., and Järvi, L.: Seasonal surface urban energy balance and wintertime stability simulated using three land-surface models in the high-latitude city Helsinki, *Q.J.R. Meteorol. Soc.*, 142, 401–417, <https://doi.org/10.1002/qj.2659>, 2016.
- 605 Kent, C. W., Grimmond, S., Barlow, J., Gatey, D., Kotthaus, S., Lindberg, F., and Halios, C. H.: Evaluation of Urban Local-Scale Aerodynamic Parameters: Implications for the Vertical Profile of Wind Speed and for Source Areas, *Boundary-Layer Meteorol*, 164, 183–213, <https://doi.org/10.1007/s10546-017-0248-z>, 2017.
- Kokkonen, T. V., Grimmond, C. S. B., Rätty, O., Ward, H. C., Christen, A., Oke, T. R., Kotthaus, S., and Järvi, L.: Sensitivity of Surface Urban Energy and Water Balance Scheme (SUEWS) to downscaling of reanalysis forcing data, *Urban Climate*, 23, 36–52, <https://doi.org/10.1016/j.uclim.2017.05.001>, 2018.
- 610 Kotthaus, S. and Grimmond, C. S. B.: Identification of Micro-scale Anthropogenic CO₂, heat and moisture sources – Processing eddy covariance fluxes for a dense urban environment, *Atmospheric Environment*, 57, 301–316, <https://doi.org/10.1016/j.atmosenv.2012.04.024>, 2012.
- Kotthaus, S. and Grimmond, C. S. B.: Energy exchange in a dense urban environment – Part I: Temporal variability of long-term observations in central London, *Urban Climate*, 10, Part 2, 261–280, <https://doi.org/10.1016/j.uclim.2013.10.002>, 2014a.
- Kotthaus, S. and Grimmond, C. S. B.: Energy exchange in a dense urban environment – Part II: Impact of spatial heterogeneity of the surface, *Urban Climate*, 10, Part 2, 281–307, <https://doi.org/10.1016/j.uclim.2013.10.001>, 2014b.
- 615 Lipson, M.: Code to process “Harmonized gap-filled datasets from 20 urban flux tower sites” for the Urban-PLUMBER projects, Zenodo, <https://doi.org/10.5281/ZENODO.6590942>, 2022a.
- Lipson, M.: Code to produce figures in the manuscript: “Harmonized, gap-filled dataset from 20 urban flux tower sites,” Zenodo, <https://doi.org/10.5281/ZENODO.6590941>, 2022b.
- Lipson, M., Grimmond, S., and Best, M.: A new multi-site evaluation project for modelling in urban areas, *Urban Climate News*, 15–16, 2020a.
- 620 Lipson, M., Grimmond, S., Best, M. J., Abramowitz, G., Pitman, A. J., and Ward, H. C.: Urban-PLUMBER: A new evaluation and benchmarking project for land surface models in urban areas, EGU General Assembly 2020, event: EGU2020DOI: 10.5194/egusphere-egu2020-20987, <https://doi.org/10.5194/egusphere-egu2020-20987>, 2020b.
- Lipson, M., Grimmond, S., Best, M. J., Abramowitz, G., and Pitman, A. J.: Urban-PLUMBER—Evaluation and Benchmarking of Land Surface Models in Urban Areas, 100th American Meteorological Society Annual Meeting, 2020c.
- 625 Lipson, M., Grimmond, S., and Best, M.: Protocol for observational data used in Urban-PLUMBER, <https://doi.org/10.5281/ZENODO.5518278>, 2021.
- Lipson, M., Grimmond, S., Best, M., Chow, W., Christen, A., Chrysoulakis, N., Coutts, A., Crawford, B., Earl, S., Evans, J., Fortuniak, K., Heusinkveld, B. G., Hong, J.-W., Hong, J., Järvi, L., Jo, S., Kim, Y.-H., Kotthaus, S., Lee, K., Masson, V., McFadden, J. P., Michels, O., Pawlak, W., Roth, M., Sugawara, H., Tapper, N., Velasco, E., and Ward, H. C.: Site data archive for “Harmonized gap-filled dataset from 20 urban flux tower sites” for the Urban-PLUMBER project (v0.92), <https://doi.org/10.5281/ZENODO.6590886>, 2022.



- 630 Urban-PLUMBER: A multi-site model evaluation project for urban areas - Project Home: <https://urban-plumber.github.io/>, last access: 1 July 2021.
Macdonald, R. W., Griffiths, R. F., and Hall, D. J.: An improved method for the estimation of surface roughness of obstacle arrays, *Atmospheric Environment*, 32, 1857–1864, [https://doi.org/10.1016/S1352-2310\(97\)00403-2](https://doi.org/10.1016/S1352-2310(97)00403-2), 1998.
Martens, B., Schumacher, D. L., Wouters, H., Muñoz-Sabater, J., Verhoest, N. E. C., and Miralles, D. G.: Evaluating the land-surface energy partitioning in ERA5, 13, 4159–4181, <https://doi.org/10.5194/gmd-13-4159-2020>, 2020.
- 635 Masson, V., Gomes, L., Pigeon, G., Lioussé, C., Pont, V., Lagouarde, J.-P., Voogt, J., Salmond, J., Oke, T. R., Hidalgo, J., Legain, D., Garrouste, O., Lac, C., Connan, O., Briottet, X., Lachérade, S., and Tulet, P.: The Canopy and Aerosol Particles Interactions in Toulouse Urban Layer (CAPITOU) experiment, *Meteorol Atmos Phys*, 102, 135, <https://doi.org/10.1007/s00703-008-0289-4>, 2008.
Masson, V., Heldens, W., Bocher, E., Bonhomme, M., Bucher, B., Burmeister, C., de Munck, C., Esch, T., Hidalgo, J., Kanani-Sühring, F., Kwok, Y.-T., Lemonsu, A., Lévy, J.-P., Maronga, B., Pavlik, D., Petit, G., See, L., Schoetter, R., Tornay, N., Votsis, A., and Zeidler, J.: City-descriptive input data for urban climate models: Model requirements, data sources and challenges, *Urban Climate*, 31, 100536, <https://doi.org/10.1016/j.uclim.2019.100536>, 2020.
- 640 McNorton, J. R., Arduini, G., Bousseret, N., Agustí-Panareda, A., Balsamo, G., Boussetta, S., Choulga, M., Hadade, I., and Hogan, R. J.: An Urban Scheme for the ECMWF Integrated Forecasting System: Single-Column and Global Offline Application, 13, e2020MS002375, <https://doi.org/10.1029/2020MS002375>, 2021.
- 645 Menard, C. B., Essery, R., Krinner, G., Arduini, G., Bartlett, P., Boone, A., Brutel-Vuilmet, C., Burke, E., Cuntz, M., Dai, Y., Decharme, B., Dutra, E., Fang, X., Fierz, C., Gusev, Y., Hagemann, S., Haverd, V., Kim, H., Lafaysse, M., Marke, T., Nasonova, O., Nitta, T., Niwano, M., Pomeroy, J., Schädler, G., Semenov, V. A., Smirnova, T., Strasser, U., Swenson, S., Turkov, D., Wever, N., and Yuan, H.: Scientific and Human Errors in a Snow Model Intercomparison, 102, E61–E79, <https://doi.org/10.1175/BAMS-D-19-0329.1>, 2021.
- 650 Menne, M. J., Durre, I., Vose, R. S., Gleason, B. E., and Houston, T. G.: An Overview of the Global Historical Climatology Network-Daily Database, 29, 897–910, <https://doi.org/10.1175/JTECH-D-11-00103.1>, 2012.
Menzer, O. and McFadden, J. P.: Statistical partitioning of a three-year time series of direct urban net CO₂ flux measurements into biogenic and anthropogenic components, *Atmospheric Environment*, 170, 319–333, <https://doi.org/10.1016/j.atmosenv.2017.09.049>, 2017.
New, M., Hulme, M., and Jones, P.: Representing Twentieth-Century Space–Time Climate Variability. Part I: Development of a 1961–90 Mean Monthly Terrestrial Climatology, 12, 829–856, [https://doi.org/10.1175/1520-0442\(1999\)012<0829:RTCSTC>2.0.CO;2](https://doi.org/10.1175/1520-0442(1999)012<0829:RTCSTC>2.0.CO;2), 1999.
- 655 Nogueira, M.: Inter-comparison of ERA-5, ERA-interim and GPCP rainfall over the last 40 years: Process-based analysis of systematic and random differences, *Journal of Hydrology*, 583, 124632, <https://doi.org/10.1016/j.jhydrol.2020.124632>, 2020.
Nordbo, A., Järvi, L., Haapanala, S., Moilanen, J., and Vesala, T.: Intra-City Variation in Urban Morphology and Turbulence Structure in Helsinki, Finland, *Boundary-Layer Meteorol*, 146, 469–496, <https://doi.org/10.1007/s10546-012-9773-y>, 2013.
- 660 Novick, K. A., Biederman, J. A., Desai, A. R., Litvak, M. E., Moore, D. J. P., Scott, R. L., and Torn, M. S.: The AmeriFlux network: A coalition of the willing, *Agricultural and Forest Meteorology*, 249, 444–456, <https://doi.org/10.1016/j.agrformet.2017.10.009>, 2018.
Offerle, B., Jonsson, P., Eliasson, I., and Grimmond, C. S. B.: Urban Modification of the Surface Energy Balance in the West African Sahel: Ouagadougou, Burkina Faso, 18, 3983–3995, 2005.
Oke, T. R.: The urban energy balance, 12, 471–508, <https://doi.org/10.1177/030913338801200401>, 1988.
Oke, T. R., Mills, G., Christen, A., and Voogt, J. A.: *Urban Climates*, Cambridge University Press, <https://doi.org/10.1017/9781139016476>, 2017.
- 665 Pastorello, G., Trotta, C., Canfora, E., Chu, H., Christianson, D., Cheah, Y.-W., Poindexter, C., Chen, J., Elbashandy, A., Humphrey, M., Isaac, P., Polidori, D., Reichstein, M., Ribeca, A., van Ingen, C., Vuichard, N., Zhang, L., Amiro, B., Ammann, C., Arain, M. A., Ardö, J., Arkebauer, T., Arndt, S. K., Arriga, N., Aubinet, M., Aurela, M., Baldocchi, D., Barr, A., Beamesderfer, E., Marchesini, L. B., Bergeron, O., Beringer, J., Bernhofer, C., Berveiller, D., Billesbach, D., Black, T. A., Blanken, P. D., Bohrer, G., Boike, J., Bolstad, P. V., Bonal, D., Bonnefond, J.-M., Bowling, D. R., Bracho, R., Brodeur, J., Brümmer, C., Buchmann, N., Burban, B., Burns, S. P., Buysse, P., Cale, P., Cavagna, M., Cellier, P., Chen, S., Chini, I., Christensen, T. R., Cleverly, J., Collalti, A., Consalvo, C., Cook, B. D., Cook, D., Coursolle, C., Cremonese, E., Curtis, P. S., D’Andrea, E., da Rocha, H., Dai, X., Davis, K. J., Cinti, B. D., Grandcourt, A. de Ligne, A. D., De Oliveira, R. C., Delpierre, N., Desai, A. R., Di Bella, C. M., Tommasi, P. di Dolman, H., Domingo, F., Dong, G., Dore, S., Duce, P., Dufrêne, E., Dunn, A., Dušek, J., Eamus, D., Eichelmann, U., ElKhidir, H. A. M., Eugster, W., Ewenz, C. M., Ewers, B., Famulari, D., Fares, S., Feigenwinter, I., Feitz, A., Fensholt, R., Filippa, G., Fischer, M., Frank, J., Galvagno, M., et al.: The FLUXNET2015 dataset and the ONEFlux processing pipeline for eddy covariance data, *Sci Data*, 7, 225, <https://doi.org/10.1038/s41597-020-0534-3>, 2020.
- 675 Pawlak, W., Fortuniak, K., and Siedlecki, M.: Carbon dioxide flux in the centre of Łódź, Poland—analysis of a 2-year eddy covariance measurement data set, 31, 232–243, <https://doi.org/10.1002/joc.2247>, 2011.
Peters, E. B., Hiller, R. V., and McFadden, J. P.: Seasonal contributions of vegetation types to suburban evapotranspiration, 116, <https://doi.org/10.1029/2010JG001463>, 2011.
- 680 Porson, A., Clark, P. A., Harman, I. N., Best, M. J., and Belcher, S. E.: Implementation of a new urban energy budget scheme in the MetUM. Part I: Description and idealized simulations, 136, 1514–1529, <https://doi.org/10.1002/qj.668>, 2010.



- Rew, R., Davis, G., Emmerson, S., Cormack, C., Caron, J., Pincus, R., Hartnett, E., Heimbigner, D., Appel, L., and Fisher, W.: Unidata NetCDF, UCAR/NCAR - Unidata, <https://doi.org/10.5065/D6H70CW6>, 1989.
- Roth, M., Jansson, C., and Velasco, E.: Multi-year energy balance and carbon dioxide fluxes over a residential neighbourhood in a tropical city, *Int. J. Climatol.*, 37, 2679–2698, <https://doi.org/10.1002/joc.4873>, 2017.
- 685 Schmid, H. P., Grimmond, C. S. B., Cropley, F., Offerle, B., and Su, H.-B.: Measurements of CO₂ and energy fluxes over a mixed hardwood forest in the mid-western United States, *Agricultural and Forest Meteorology*, 103, 357–374, [https://doi.org/10.1016/S0168-1923\(00\)00140-4](https://doi.org/10.1016/S0168-1923(00)00140-4), 2000.
- Shi, Y., Zhang, Y., and Li, R.: Local-Scale Urban Energy Balance Observation under Various Sky Conditions in a Humid Subtropical Region, *J. Appl. Meteor. Climatol.*, 58, 1573–1591, <https://doi.org/10.1175/JAMC-D-18-0273.1>, 2019.
- 690 Stagakis, S., Chrysoulakis, N., Spyridakis, N., Feigenwinter, C., and Vogt, R.: Eddy Covariance measurements and source partitioning of CO₂ emissions in an urban environment: Application for Heraklion, Greece, *Atmospheric Environment*, 201, 278–292, <https://doi.org/10.1016/j.atmosenv.2019.01.009>, 2019.
- Tang, Y., Sun, T., Luo, Z., Omidvar, H., Theeuwes, N., Xie, X., Xiong, J., Yao, R., and Grimmond, S.: Urban meteorological forcing data for building energy simulations, *Building and Environment*, 204, 108088, <https://doi.org/10.1016/j.buildenv.2021.108088>, 2021.
- Ukkola, A. M., Houghton, N., Kauwe, M. G. D., Abramowitz, G., and Pitman, A. J.: FluxnetLSM R package (v1.0): a community tool for processing FLUXNET data for use in land surface modelling, *10*, 3379–3390, <https://doi.org/10.5194/gmd-10-3379-2017>, 2017.
- 695 Ukkola, A. M., Abramowitz, G., and De Kauwe, M. G.: A flux tower dataset tailored for land model evaluation, *14*, 449–461, <https://doi.org/10.5194/essd-14-449-2022>, 2022.
- UN: World Urbanization Prospects: The 2018 Revision, Online Edition, United Nations, Department of Economic and Social Affairs, Population Division, 2018.
- 700 Valentini, R.: EUROFLUX: An Integrated Network for Studying the Long-Term Responses of Biospheric Exchanges of Carbon, Water, and Energy of European Forests, in: *Fluxes of Carbon, Water and Energy of European Forests*, edited by: Valentini, R., Springer, Berlin, Heidelberg, 1–8, https://doi.org/10.1007/978-3-662-05171-9_1, 2003.
- Varquez, A. C. G., Kiyomoto, S., Khanh, D. N., and Kanda, M.: Global 1-km present and future hourly anthropogenic heat flux, *8*, 64, <https://doi.org/10.1038/s41597-021-00850-w>, 2021.
- 705 Velasco, E. and Roth, M.: Cities as Net Sources of CO₂: Review of Atmospheric CO₂ Exchange in Urban Environments Measured by Eddy Covariance Technique, *4*, 1238–1259, <https://doi.org/10.1111/j.1749-8198.2010.00384.x>, 2010.
- Velasco, E., Pressley, S., Grivicke, R., Allwine, E., Molina, L. T., and Lamb, B.: Energy balance in urban Mexico City: observation and parameterization during the MILAGRO/MCMA-2006 field campaign, *Theor Appl Climatol*, 103, 501–517, <https://doi.org/10.1007/s00704-010-0314-7>, 2011.
- Velasco, E., Roth, M., Tan, S. H., Quak, M., Nabarro, S. D. A., and Norford, L.: The role of vegetation in the CO₂ flux from a tropical urban neighbourhood, *13*, 10185–10202, <https://doi.org/10.5194/acp-13-10185-2013>, 2013.
- 710 Velasco, E., Perrusquia, R., Jiménez, E., Hernández, F., Camacho, P., Rodríguez, S., Retama, A., and Molina, L. T.: Sources and sinks of carbon dioxide in a neighborhood of Mexico City, *Atmospheric Environment*, 97, 226–238, <https://doi.org/10.1016/j.atmosenv.2014.08.018>, 2014.
- Vitale, D., Fratini, G., Bilancia, M., Nicolini, G., Sabbatini, S., and Papale, D.: A robust data cleaning procedure for eddy covariance flux measurements, *17*, 1367–1391, <https://doi.org/10.5194/bg-17-1367-2020>, 2020.
- 715 Vuichard, N. and Papale, D.: Filling the gaps in meteorological continuous data measured at FLUXNET sites with ERA-Interim reanalysis, *7*, <https://doi.org/10.5194/essd-7-157-2015>, 2015.
- Ward, H. C., Evans, J. G., and Grimmond, C. S. B.: Multi-season eddy covariance observations of energy, water and carbon fluxes over a suburban area in Swindon, UK, *13*, 4645–4666, <https://doi.org/10.5194/acp-13-4645-2013>, 2013.
- 720 Weedon, G. P., Gomes, S., Viterbo, P., Shuttleworth, W. J., Blyth, E., Österle, H., Adam, J. C., Bellouin, N., Boucher, O., and Best, M.: Creation of the WATCH Forcing Data and Its Use to Assess Global and Regional Reference Crop Evaporation over Land during the Twentieth Century, *J. Hydrometeor.*, 12, 823–848, <https://doi.org/10.1175/2011JHM1369.1>, 2011.
- World Meteorological Organization: Guide to meteorological instruments and methods of observation., World Meteorological Organization, Geneva, Switzerland, 2008.
- Yamamoto, S., Saigusa, N., Gamo, M., Fujinuma, Y., Inoue, G., and Hirano, T.: Findings through the AsiaFlux network and a view toward the future, *J. Geogr. Sci.*, 15, 142–148, <https://doi.org/10.1007/BF02872679>, 2005.